Trace element systematics in cold seep carbonates and associated lipid compounds

Xudong Wang, Germain Bayon, Jung-Hyun Kim, Dong-Hun Lee, Dahae Kim, Bleuenn Guéguen, Marie-Laure Rouget, Jean-Alix J-A Barrat, Laurent Toffin, Dong Feng

▶ **To cite this version:**

Xudong Wang, Germain Bayon, Jung-Hyun Kim, Dong-Hun Lee, Dahae Kim, et al.. Trace element systematics in cold seep carbonates and associated lipid compounds. Chemical Geology, 2019, 528, pp.119277 -. ⟨10.1016/j.chemgeo.2019.119277⟩. ⟨hal-03487202⟩

HAL Id: hal-03487202

https://hal.science/hal-03487202v1

Submitted on 20 Dec 2021

HAL is a multi-disciplinary open access archive for the deposit and dissemination of scientific research documents, whether they are published or not. The documents may come from teaching and research institutions in France or abroad, or from public or private research centers.

L'archive ouverte pluridisciplinaire **HAL**, est destinée au dépôt et à la diffusion de documents scientifiques de niveau recherche, publiés ou non, émanant des établissements d'enseignement et de recherche français ou étrangers, des laboratoires publics ou privés.

Distributed under a Creative Commons CC BY-NC 4.0 - Attribution - Non-commercial use - International License

Version of Record: https://www.sciencedirect.com/science/article/pii/S0009254119303845
Manuscript_43dbdbfc0b6e45a9725b00f35e43313e

Trace element systematics in cold seep carbonates and associated lipid compounds

Xudong Wang[a,b,g,h], Germain Bayon[b], Jung-Hyun Kim[c], Dong-Hun Lee[d], Dahae Kim[c], Bleuenn Guéguen[e], Marie-Laure Rouget[e], Jean-Alix Barrat[e], Laurent Toffin[f], Dong Feng[a,g]

[a] Key Laboratory of Ocean and Marginal Sea Geology, South China Sea Institute of Oceanology, Chinese Academy of Sciences, Guangzhou 510301, China
[b] IFREMER, Marine Geosciences Unit F-29280 Plouzané, France
[c] KOPRI Korea Polar Research Institute, 26 Songdomirae-ro, Yeonsu-gu, Incheon 21990, South Korea
[d] Hanyang University, 55 Hanyangdaehak-ro, Sangrok-gu, Ansan 15588, Republic of Korea
[e] Laboratoire Géosciences Océan, Université de Bretagne Occidentale et Institut Universitaire Européen de la Mer, Place Nicolas Copernic, 29280 Plouzané, France
[f] IFREMER, UMR6197, Laboratoire Microbiologie des Environnements Extrêmes, F-29280 Plouzané, France
[g] Innovation Academy of South China Sea Ecology and Environmental Engineering, Chinese Academy of Sciences, Guangzhou 510301, China
[h] University of Chinese Academy of Sciences, Beijing 100049, China

Corresponding authors:
Germain Bayon (gbayon@ifremer.fr), Dong Feng (feng@scsio.ac.cn),

Word count: 7,298

Revised manuscript submitted to Chemical Geology

© 2019 published by Elsevier. This manuscript is made available under the CC BY NC user license
https://creativecommons.org/licenses/by-nc/4.0/

Abstract

Seeping of methane-rich fluids at submarine cold seeps drives intense microbial activity and precipitation of authigenic carbonates. Some trace elements play an important role in the biogeochemical processes operating at cold seeps, especially as specific enzymatic co-factors related to methanogenesis and the anaerobic oxidation of methane (AOM). However, it is unclear whether microbial trace metal utilization can be traced by the geochemical composition of seep carbonates. In this study, we analyzed a series of authigenic carbonate samples recovered from various seep settings worldwide and report for the first time trace element concentrations for total lipid fractions, combined with biomarker analyses and determination of elemental abundances in associated inorganic mineral phases (carbonate phases, sulfides, organic compounds and detrital fractions). Our results indicate marked enrichments of Co, Ni, Cu, Mo and W in the archaeal and bacterial lipids associated with authigenic carbonates, which can all be ascribed to previously identified enzymatic pathways. In addition to the microbial communities involved in AOM, which most likely control specific lipid-bound enrichments of Co, Ni, Mo and W in seep carbonates, Cu was found to display higher concentrations in the lipid fractions extracted from a few authigenic carbonate samples formed closer to the sediment-water interface, hence possibly related to the presence of aerobic methane-oxidizing bacterial assemblages in the near seafloor environment. While the above mentioned trace metals are relatively enriched in all studied inorganic and organic fractions, the very low W concentrations measured in carbonate phases, combined with their pronounced enrichment in associated lipid fractions and inferred microbial requirement, suggest that tungsten depletion in pore waters could possibly act as a limiting factor on AOM at cold seeps. Finally, two other trace elements (Li and Ti) also displayed particular enrichments in studied lipid fractions, which, despite no reported evidence, could possibly indicate that they are also involved as metalloenzymes in microbial methane oxidation processes at cold seeps.

Key words: seep carbonate; lipid compounds; trace elements; tungsten; nickel; cobalt; molybdenum

1. Introduction

The seepage of methane-rich fluids at ocean margins sustains abundant chemosynthetic seafloor ecosystems, which rely on the use of reduced chemical compounds (Levin, 2005). Fluid seepage is accompanied by intense microbial activity at cold seeps, leading to precipitation of authigenic minerals, such as carbonates and sulfides, and development of microbial mats close to the seafloor (Sibuet and Olu, 1998; Peckmann et al., 2001; Joye et al., 2004). Microbial communities prospering in cold seep environments support the highest biomass in deep-sea ecosystems, with up to 10^{12} cells per cm^3 (Michaelis et al., 2002). The dominant microbial processes at cold seeps is the anaerobic oxidation of methane (AOM) coupled to sulfate reduction. Until recently, it was generally thought that AOM was mainly coupled with sulfate reduction in anoxic sediments, both processes being driven by a consortium of archaea and bacteria assemblages, respectively (e.g. Boetius et al., 2000). However, over the past few years, several studies have demonstrated that microorganisms could also use nitrate or metal oxides to promote methane oxidation at cold seeps (Raghoebarsing et al., 2006; Beal et al., 2009; Scheller et al., 2010; Glass et al., 2014). Manganese

(Mn) and iron (Fe)-rich oxyhydroxides have been identified as electron acceptors for AOM (Beal et al., 2009), but other trace metals, such as nickel (Ni), cobalt, (Co), molybdenum (Mo) and tungsten (W) are also involved in methane oxidation processes as enzymatic co-factors (Krüger et al., 2003; Glass et al., 2014). Trace metals are also suspected to have played key roles in the long-term evolution of microbial activity through geologic time (Anbar, 2008; Konhauser et al., 2009; Reinhard et al., 2013). For example, an important drop in dissolved Ni concentrations in Precambrian oceans after about 2.5 Ga, as a consequence of the progressive decrease in the production of Ni-rich volcanic rocks (komatiites) on Earth, would have led to reduced activity of methanogenic microbes, with possibly global impact on the composition of the atmosphere (Konhauser et al., 2009). To date, however, and despite their potential importance in AOM, very little is known about the utility of trace elements for microbial activity and metabolism at cold seeps.

Trace metals are essential in biological systems, playing key roles in microbially-driven biogeochemical processes. In addition to iron, other transition metals (Zn, Mn, Co, Ni, Cu, V, Mo and W) have been identified in proteins and enzymes involved in the metabolism of sulfate-reducing bacteria or methanogenic and methanotrophic archaea (e.g. Scherer et al., 1983; Krüger et al., 2003; Barton et al., 2007; Scheller et al., 2010; Glass and Orphan, 2012; Glass et al., 2014; 2018). Amongst trace metals, Ni appears to play a particularly important role in anaerobic methanotrophy and methanogenesis (Krüger et al., 2003; Scheller et al., 2010; Thauer et al., 2010). The microbial communities involved in AOM also utilize other essential trace metals, such as Co, W and Mo (e.g. Glass et al., 2014; 2018). Many of these findings have been obtained from culture experiments, but little is known about how microbial activity at cold seeps may be affected by changes in trace metal bioavailability from one site to another. Transition metals can be intensively scavenged during precipitation of authigenic minerals, such as sulfides and carbonates in methane seepage areas (Bayon et al., 2011a; Lemaitre et al., 2014), which can severely reduce their availability to microbial communities (Glass and Orphan, 2012). Recent investigations have also suggested that light rare earth elements (REE) could be essential for methanotrophs as co-factors in the methanol dehydrogenase enzyme (Pol et al., 2014; Jahn et al., 2018; Picone and den Camp, 2019). This previously unsuspected biological role of REE for methanotrophic and methylotrophic bacteria was also demonstrated in a recent study that investigated the methane plumes emitted in the Gulf of Mexico following the Deepwater Horizon blowout, which revealed significant depletion of light REE (La, Ce, Pr, and Nd) relative to the surrounding seawater (Scheller et al., 2017).

At submarine methane seeps, authigenic carbonates are a by-product of microbially-mediated AOM (Aloisi et al., 2000; 2002), which can hence provide unique information on past seepage activity and associated environmental parameters (Feng et al., 2015). Extensive work has been conducted on the geochemistry of authigenic carbonates and associated sediments, in both modern and ancient seep settings. Previous studies have focused on both conventional and non-conventional stable isotopes and radiogenic isotopes (including U-Th dating methods) to provide constraints on both fluid sources and the timing of fluid seepage events at ocean margins (Peckmann et al., 2001; Pierre and Fouquet, 2007; Ge and Jiang, 2013; Bayon et al., 2015; Hu et al., 2015a; Sun et al., 2015; Lu et al., 2017).

Trace elements in seep carbonates have been mostly used as proxies for the source of fluids, but also to provide information on redox conditions. Both carbonates and associated sediments at methane seeps display relatively high elemental concentrations, suggesting that they act as a sink for many trace elements, such as Mo and rare earth elements (Sato et al., 2012; Lemaitre et al., 2014; Hu et al., 2015b). It is generally assumed that trace element distribution patterns in authigenic carbonates reflect the composition of ambient pore waters. However, fractionation of REE can occur upon carbonate precipitation, in response to changing carbonate alkalinity levels in pore waters, which affect REE complexation by organic and carbonate ligands (Himmler et al., 2010; Rongemaille et al., 2011). The degree of Ce enrichment or depletion in modern and ancient seep carbonates, relative to its trivalent REE neighbors (the so-called Ce-anomaly), has been also used as a paleo-redox tracer (Feng et al., 2009).

Comparatively, there have been very few studies dedicated to trace elements in organic compounds at cold seeps. Freslon et al. (2014) reported REE concentrations for organic compounds chemically leached from a series of marine sediment samples, including sediments recovered from active seep sites worldwide, showing strong REE enrichments in cold seep sediments. This study suggested that a significant fraction of sedimentary organic matter at these sites was derived from chemosynthetic processes recycling REE-enriched pore waters. Over the past decades, lipid biomarker analysis of seep carbonates has provided a wealth of information on the nature of microbial communities involved in carbonate precipitation (e.g. Aloisi et al., 2002; Himmler et al., 2015; Guan et al., 2016). However, to the best of our knowledge, the trace element geochemistry of lipids preserved in authigenic carbonates has never been investigated so far.

In this study, we aimed at characterizing the trace element geochemistry of lipids preserved in authigenic carbonates, in order to provide independent information on the utility of trace metals to microbial activity at methane seeps. In contrast to the trace element signatures preserved by inorganic phases in cold seep carbonates, which mostly reflect the composition of ambient pore waters and local redox conditions (Hu et al., 2015b), our working hypothesis is that any particular elemental enrichments/anomalies in the lipid fractions reflect trace metal requirements for microbial metabolism. To this purpose, we have analysed a series of authigenic carbonate samples from various active seeps worldwide, reporting trace element data for both carbonate and lipid fractions. Our approach combines biomarker and inorganic element analyses of total lipid fractions extracted from a series of carbonate crusts, together with determination of trace element contents in associated mineral phases (carbonates, sulfides and organic compounds, detrital fractions), separated by sequential chemical leaching. The aim of this study was to detect specific enrichments that would be indicative of preferential metal utilization by microorganisms.

2. Materials and methods

2.1. Sample preparation

A total of 19 seep carbonate samples from five different active seepage areas worldwide (Congo fan, Nile deep-sea fan, Niger fan, Eastern Mediterranean Sea, Gulf of Mexico) were analyzed (Fig. 1). Most of these samples have been previously characterized for carbonate mineralogy and/or

stable isotopes (Table 1; see references therein). For clarity, note that we re-labelled the name of the samples in this study (Fig. 1; Table 1).

2.2. Pretreatment procedures

Carbonate chips were first cleaned with ultrapure Milli-Q (MQ) water and dried, prior to being crushed into powder using an agate and mortar. Samples were split into two aliquots of about 5 g each for lipid biomarker extraction and analyses at the Korea Polar Research Institute (KOPRI) and sequential chemical leaching at IFREMER, respectively.

Upon formation at cold seeps, authigenic carbonates can incorporate substantial amounts of sulfide and detrital minerals from the surrounding sediment, in addition to the various organic compounds related to AOM. Previous studies have shown that even a small proportion of detrital contamination can significantly modify trace element abundances in carbonates (Nance and Taylor, 1976; Nothdurft et al., 2004, Frimmel, 2009). Therefore, selective chemical leaching methods are required for investigating the geochemistry of relatively pure carbonate and organic phases, without contamination from detrital and sulfide minerals (Bayon et al., 2002; Rongemaille et al., 2011; Freslon et al., 2014). In this study, we used a sequential leaching procedure adapted from Chao and Sanzalone (1977), Freslon et al. (2014) and Tachikawa et al. (2014), resulting in the following sequence of leaching steps: 1) stepwise addition of 1M acetic acid (AA), to extract a pure fraction of the most labile carbonate phases, such as aragonite and calcite; 2) 0.25M HCl, to remove most carbonate minerals; 3) 5% hydrogen peroxide (H_2O_2), to extract organic compounds (and possibly some sulfide minerals); 4) 3M HNO_3 to leach out pyrite minerals (and presumably any residual carbonate and organic phases); 5) digestion of detrital silicate minerals using concentrated HF + HCl.

For the first leaching step, about 50 mg of powdered carbonate samples were placed into an acid-cleaned 15 ml polyethylene centrifuge tube, together with 500 µl ultrapure MQ water. After addition of a Tm spike (see details below), carbonates were slowly dissolved with stepwise (100 µl) addition of ultraclean 1M AA solution. The next 100 µl aliquot was added once the bubbling has ceased; this step being repeated until addition of a total of 1 ml 1M AA, hence corresponding to a resulting leaching solution of about 3.8 wt%. This gentle leaching step was initially developed for measuring neodymium (Nd) isotopic ratios in foraminifera (Tachikawa et al., 2014). It ensures partial dissolution of the most soluble carbonate phases (aragonite, calcite) with limited contamination from silicate and sulfide minerals. The tube was then centrifuged at 3800 rpm for 4 minutes, and the supernatant was transferred into a cleaned polytetrafluoroethylene (PTFE) vial, prior to evaporation and preparation for ICP-MS analyses.

Next, a four-stage sequential leaching procedure was conducted on our series of carbonate samples, starting from about 500 mg of bulk powdered samples. Following a protocol adapted from Freslon et al. (2014), the most soluble carbonate phases were first dissolved using 0.25M HCl in a PTFE vial left at room temperature for 3 hours. After centrifugation of the supernatant, this leaching step was repeated once, and the remaining residue was rinsed twice with ultrapure MQ water, and dried overnight in the oven.

The remaining dried residues were weighed, crushed, and placed into corresponding PTFE vials. The next leaching step corresponded to the addition of a mixed solution of 5% H_2O_2 + 0.01M HNO_3, together with Tm spike, in order to oxidize organic matter (and possibly the easily dissolvable sulfide phases; Dold, 2003). The vials were placed on a mechanical shaker and left at room temperature for 48 hours. The solutions were centrifuged at 3500 rpm for 3 min and the supernatants were transferred into acid-cleaned 15 ml centrifuge tubes after filtration using high-density polyethylene (HDPE) 0.2 µm filters. After evaporation onto the hot plate, the organic-rich samples were digested overnight with concentrated nitric (140°C), prior to being evaporated again and prepared for ICP-MS analyses.

Next, the residues left after the H_2O_2 leaching step were rinsed with ultrapure MQ water, dried overnight, crushed and weighed. The next leaching step was performed using 3M HNO_3, aiming at dissolving a substantial fraction of sulfide minerals (Chao and Sanzalone, 1977), but also, presumably, any residual carbonate and organic phases that would have been left after the 0.25M HCl and 5% H_2O_2 steps, together with probably some silicate minerals. Chao and Sanzalone (1977) investigated various chemical treatments for dissolving primary sulfide minerals in sediments, showing that the use of moderately diluted HNO_3 solutions was quite effective for dissolving pyrite, hence our decision to use 3M HNO_3 for this leaching step. After addition of a Tm spike, 3M HNO_3 was added to the samples and left on a mechanical shaker overnight. The leachates were separated by centrifugation (3800 rpm for 4 min) and transferred into an acid cleaned Teflon vial prior to preparation for ICP-MS analyses. The residues were rinsed with ultrapure MQ water, dried and crushed. Finally, about 15 mg of the final residual fractions were digested on the hotplate (140°C for 5 days) with concentrated HF and HCl.

2.3. ICP-MS analysis

All trace element analyses were performed at the Pôle Spectrométrie Océan (Brest, France) on an Element XR ICP-MS. Polyatomic oxide and hydroxide interferences on the REE were corrected using oxide formation rates determined by analyzing solutions of MQ-H_2O, Ba + Ce, Pr + Nd and Sm + Tb at the beginning of each measurement session and applied to all samples. Elemental concentrations were calculated using the Tm addition method (Barrat et al., 1996; Bayon et al., 2009). Over recent years, this method has been successfully applied to and validated for a wide range of geological samples, including detrital and organic sediments (Freslon et al., 2014; Bayon et al., 2015), carbonates (Rongemaille et al., 2011), seawater (Bayon et al., 2011b; Freslon et al., 2011). Briefly, raw trace element data were calibrated against an unspiked (no added Tm) BHVO-2 reference solution run after every three samples to correct for instrumental drift. The BHVO-2 values used for the calculations (Barrat et al., 2012; Jochum et al., 2016) are given in Table 1. Trace element abundances in the samples are then calculated using the mass of sample spiked with Tm and the amount of Tm added. The internal precision on all measurements was generally better than 5%. Repeated analyses of the JLs-1 (Triassic limestone) reference material were also performed, with a precision of < 10% for most trace elements (Table 2), except for Li (11.8% RSD), Ti (61% RSD) and Zr (17% RSD). Due to high Ba/REE ratios, several carbonate samples (including JLs-1) analyzed displayed anomalously high Eu (and to a lesser extent Gd) concentrations as a result of under-corrected interferences, hence these two elements were not reported.

2.4. Lipid biomarker analysis

Detailed procedures for lipid biomarker analyses were previously described by Lee et al. (2018). Briefly, total lipid fractions were extracted 3 times with dichloromethane (DCM):methanol (MeOH) (2:1). One-half of the total lipid extract (TLE) was dried over anhydrous Na_2SO_4 and treated with tetrabutylammonium sulfite reagent to remove elemental sulfur. The TLE was chromatographically separated into apolar and polar fractions over an Al_2O_3 (activated for 2 h at 150°C) column. The apolar fraction was eluted using hexane:DCM (9:1), and 40 µL of 5α-androstane (10 µg mL-1) was added as an internal standard. The polar fraction was recovered with DCM:MeOH (1:1) as an eluent and divided into two aliquots, to which either C_{22} 7,16-diol (10 µg mL-1) or C_{19} nonadecanoic acid (10 µg mL-1) were added as an internal standard. Each aliquot was derivatized through the procedures of silylation and methylation, prior to quantification with gas chromatography (GC) and identification with gas chromatography-mass spectrometry (GC-MS). GC and GC-MS conditions were as described by Lee et al. (2018). Molecular compounds were determined by comparing their mass spectral fragmentation patterns and retention times with previously published data (e.g. Stadnitskaia et al., 2008; Lee et al., 2018).

2.5. Principal component analysis (PCA)

Based on the fractional abundances of microbial lipids, principal component analysis (PCA) was performed using R software version 3.4.2 (package information; FactoMineR) to provide a general view of the variability of the microbial lipid distributions. For the statistical analysis, gaps in the data set were filled as described by Yunker et al. (2005). Briefly, in cases when some of microbial lipids were not determined, a value of one-half of minimum value detected for that variable in the whole data was set as the limit of detection. These values then were replaced by a random number between zero and the limit of detection. Finally, samples were transformed using Z-score normalization to remove artefacts related to the large differences in concentration between samples.

3. Results

Trace element data for carbonate (1M AA leachates), sulfide-rich (3M HNO_3 leachates), detrital (HF-HCl digestion), bulk organic (5% H_2O_2 leachates) and lipid fractions are reported in Table 3 and described below in separate sections. For clarity, results are also presented as normalized values (Fig. 2 and 3), which helps identifying any particular trace element enrichment or depletion in studied mineral and organic fractions. In addition, archaeal and bacterial lipid biomarker data were presented in Table 4 and described in a separate section.

3.1. Carbonate phases (aragonite, calcite): 1M AA leachates

Studied carbonate samples display a large range of Sr concentrations (between ~300 to 15500 mg/kg). As already described previously (e.g. Jørgensen, 1992; Savard et al., 1996; Bayon et al., 2007), aragonite-rich samples are characterized by much higher Sr contents (between ~ 8000 to 15500 mg/kg), than calcite- or dolomite-dominated samples (generally < 3000 mg/kg). Other elements also display large concentration ranges, for example for Co (between 0.03 - 2.42 mg/kg), Mo (0.05 - 5.13 mg/kg) and Nd (0.10-10.3 mg/kg). Compared to the marine limestone standard

(JLs-1), cold seep carbonate samples are generally characterized by much higher trace element contents (Fig. 2a), many of them (Li, Sc, transition metals, Sr, Mo, REE , Pb and Th) being up to a few hundred times more enriched. In contrast, three elements (Ti, Ba and W) display much lower concentrations (up to 100 times depleted compared to JLs-1).

3.2. Sulfide minerals: 3M HNO_3 leachates

The concentrations for Ca in 3M HNO_3 leachates range between 37088 and 115006 mg/kg, hence being significantly lower than in 1M AA leachates. Selected trace element concentrations also display a very large range of values (between 2.0 - 36.4 mg/kg for Ti; 0.03 - 3.84 mg/kg for Co; 0.05 - 2.16 mg/kg for Mo; and 0.06 - 8.37 mg/kg for Nd). Trace element data for 3M HNO_3 leachates are normalized to the 1M AA leachate data in order to evaluate their degree of enrichment or depletion relative to corresponding carbonate phases. Apart from Ca and Sr, and to a lesser extent Mn, Ba, REE, W and U, which are generally depleted in 3M HNO_3 leachates compared to 1M AA leachates, most trace elements are enriched up to 10 times (Co, Ni, Zn, Rb, Zr, Mo, Hf, and Th) or 100 times (Ti, Cu, Pb) in the sulfide-rich leached fractions of studied carbonate samples.

3.3. Detrital silicate fractions: conc. HF+HCl acid digestion

Measured Ca concentrations for the residual silicate fractions associated with seep carbonates (between 679 - 6165 mg/kg) are much lower than in any other studied mineral/organic phases. This shows that our sequential chemical procedure was effective at quantitatively removing most carbonate material. Many trace elements generally display a relatively small range of concentrations (Table 3). Trace element abundances in residual silicate fractions can be normalized to reference shale values, such as the Post Archean Australian shale composite (PAAS; Taylor and MacLennan, 1985), in order to identify particular enrichment or depletion relative to an average bulk sediment composition. Several elements, such as Ca, Mn, Cu, Sr, Ba and Pb, are significantly depleted in the residual silicate fraction of seep carbonates relative to PAAS, but this simply reflects, at least to some extent, the fact that PAAS is a bulk reference composite sediment that also contains non-silicate phases (carbonates) enriched in these particular elements. However, a few samples display much higher PAAS-normalized concentrations for Ba and Sr (up to 30 times), which reflect the presence of barite, i.e. a common authigenic mineral at cold seeps that is resistant to most chemical leaching procedures, including digestion using concentrated HF-HCl solutions. In addition, many residual silicate fractions are also characterized by pronounced PAAS-normalized enrichments in Mo, also up to 30 times.

3.4. Bulk organic compounds: 5% H_2O_2 leachates

The 5% H_2O_2 leachates are generally characterized by very high Ca concentrations (up to ~570000 mg/kg), indicating that carbonates represent the dominant phase extracted during this leaching step. This is also reflected by the high Sr (up to 6300 mg/kg) and Mg (up to 127000 mg/kg) concentrations determined in the same solutions. As a consequence, it appears difficult to draw any conclusions regarding the partitioning of selected trace elements into the organic compounds hosted by seep carbonates. However, normalizing the 5% H_2O_2 leachate data to those obtained for 1M AA (carbonates) and 3M HNO_3 (sulfides) leachates can still help identifying some particular elements that would be more specifically associated with the organic component hosted by seep

carbonates. This is the case for at least three elements (V, Mo and W), which all show pronounced normalized-enrichments (up to a thousand times) in 5% H_2O_2 leachates (Fig. 3a and 3b). To a lesser extent, the transition metals (Co, Ni, Cu, Zn) also appear to be enriched (up to 10-100 times) in 5% H_2O_2 leachates compared to 1M AA and 3M HNO_3 leachates.

3.5. Total lipids

In contrast to the 5% H_2O_2 leachates, the extracted lipid fractions display much lower Ca concentrations (between 2270 - 51045 mg/kg, with an average of 15000 mg/kg), hence indicating limited carbonate dissolution (generally < 5 wt%). Amongst the other studied elements, Li concentrations range from 6.6 to 32.6 mg/kg; Ti from 1.1 to 29.6 mg/kg; Cu from 0.9 to 37.9 mg/kg; Mo from 0.1 to 3.0 mg/kg and W from 0.01 to 0.08 mg/kg. In comparison, REE display very low concentrations with Nd concentrations between ~0.1 and 1.0 mg/kg. Compared to the abundances determined in carbonate (1M AA) and sulfide (3M HNO_3) leachates, elemental concentrations in lipid fractions are very low for the following elements: Ca, Sc, Mn, REE, Th and U (Fig. 3c and 3d). In contrast, some trace elements, such as Li, Ti, V, Cu, Zn, Mo, and W exhibit clearly identifiable enrichments (up to 100 times) in lipids.

3.6. Microbial lipid biomarkers

Concentrations of archaeal and bacterial lipids showed large variations in studied authigenic carbonates (Table 4). For archaeal lipids, the irregular tail-to-tail isoprenoids such as crocetane, which was co-eluted with phytane, pentamethylicosane (PMI), and polyunsaturated pentamethylicosenes (PMEs) were detected, varying between 0.03 and 0.25 μg/g dry weight (dw), 0.02 to 0.25 μg/g dw, and 0.01 to 0.49 μg/g dw, respectively. Moreover, isoprenoid dialkyl glycerol diethers (isoprenoid DGDs), such as archaeol and *sn*-2-hydroxyarchaeol, were the most predominant archaeal lipids in studied samples, displaying concentration ranges between 0.01–6.97 μg/g dw, and 0.03–22.13 μg/g dw, respectively. For bacterial lipids, non-isoprenoid DGDs with anteiso pentadecyl moieties or cyclopropyl groups attached at both the *sn*-1 and *sn*-2 positions were identified, ranging from 0.01 to 1.07 μg/g dw. Among FAs detected, saturated FAs (e.g. C16:0 and C18:0) were most predominant, with the range of 0.06–1.99 μg/g dw (Table 4). Other FAs (e.g. *i*-C15:0, *ai*-C15:0, C16:1ω7, C18:1ω9 and C18:1ω7) were approximately 3 to 10 times lower in concentrations (0.01 to 0.16 μg/g dw) compared to saturated FAs.

4. Discussion

4.1. Distribution of trace elements in authigenic carbonate phases

As discussed in previous studies, the distribution of trace elements in cold seep carbonates can be controlled by various parameters, including mineralogy, composition of the fluids from which they have precipitated from, and redox conditions (Peckmann et al, 2001; Conti et al, 2004; Bayon et al, 2007; Feng et al., 2009; Ge et al, 2010). In addition to Sr, which is significantly enriched in aragonite compared to other carbonate phases (see section 3.1), U and Mn are also preferentially incorporated into aragonite- (characterized by high Sr/Ca contents) and calcite- (low Sr/Ca) dominated samples (Fig. 4a and 4b), respectively. To a large extent, the chemical composition of surrounding pore waters also plays a major role in controlling trace element distribution patterns in authigenic carbonates. This explains why many trace elements are enriched in cold seep

carbonates compared to marine bioskeletal carbonates (e.g. JLs-1 limestone; Fig. 2a). This is illustrated taking the example of the REE, which also exhibit a relationship with mineralogy in a Nd/Ca versus Sr/Ca plot (Fig. 4c). The abundance of REE in pore waters is generally much higher than in overlying bottom waters, because of various early diagenetic processes, such as the reduction of Fe-Mn oxyhydroxide phases or organic matter remineralization, which can release substantial amounts of dissolved REE within the sub-surface sediment (Haley et al., 2004). Since high-Mg authigenic carbonate minerals, such as dolomite, often form in relatively deeply buried sulfate-depleted sediment layers (typically a few meters below the seafloor) characterized by high dissolved REE contents (Soyol-Erdene and Huh, 2013), they are likely to incorporate higher amounts of REE compared to mineral phases such as aragonite, which precipitate in the near seafloor environment from less REE-enriched pore waters.

In addition to this source effect, the ubiquitous presence of anoxic conditions at cold seeps also explains why many redox sensitive elements are typically more enriched in methane-derived carbonates compared to other marine carbonate material such as JLs-1 (Fig. 2a). For instance, this is the case for redox sensitive elements like Mo, U, Ni, V, Cd, Co, and Zn, which are typically immobilized under anoxic conditions. In fact, many of these elements have been used in previous studies for providing constraints into the redox conditions of formation of carbonate minerals (Morford and Emerson, 1999; Sarkar et al., 2003). Enrichments in Mo have been reported widely in many seep carbonate samples (Central Mediterranean, Cangemi et al., 2010; Vocontian Trough, SE-France, Tribovillard et al., 2013; Gulf of Mexico, Hu et al., 2014; Northwestern South China Sea, Liang et al., 2017; Southwestern Taiwan, Wang et al., 2019). Ge et al. (2010) also found particularly high abundances of Mo, V, Co, Ni and U in authigenic carbonate samples recovered from the Shenhu and Dongsha seep areas of the South China Sea compared to marine bioskeletal carbonates.

In marked contrast, as shown in the results section, Ba, Ti and W often display much lower abundances in studied seep carbonates relative to JLs-1 (Fig. 2a). For Ba, this depletion is best explained by the fact that precipitation of authigenic barite at cold seeps acts as an effective sink for pore water Ba. While previous partitioning experiments have demonstrated that Ba is preferentially incorporated into aragonite compared to calcite (Pingitore Jr and Eastman, 1984), our results indicate instead that Ba generally exhibit higher concentrations in calcite rather than in aragonite-dominated samples (Fig. 4d). This preferential enrichment of Ba in calcite relative to aragonite is most likely controlled by the availability of Ba at the depth of mineral formation (e.g., Torres et al, 2002, 2010; Snyder et al, 2007). At methane seeps, pore water Ba concentrations markedly increase in the sediment column located below the depth of sulfate depletion, as a consequence of barite ($BaSO_4$) dissolution. The upward diffusing resulting flux of dissolved Ba is almost quantitatively precipitated into authigenic barite at the sulfate-methane transition zone (SMTZ), but a minor fraction of dissolved Ba is also likely to be incorporated into the high-Mg carbonate phases that form at the SMTZ when it is located well below the sediment-seafloor interface. In contrast, aragonite generally forms in the sulfate-rich near seafloor environment at cold seeps (Burton, 1993, Luff and Wallmann, 2003, Peckmann et al., 2009), where pore water Ba contents are presumably much lower than in the deeper methanogenic sediments, hence possibly explaining the relatively low Ba concentrations encountered in most aragonite-rich samples (Liang

et al., 2017).

The cause of Ti and W depletion in studied carbonate samples remains unclear, as these features have never been described previously in the literature, at least to the best of our knowledge. This will be the focus of a part of the discussion below, when interpreting the results obtained for the organic fractions. One hypothesis would be that these elements have been partly re-adsorbed onto residual phases during the 1M AA leaching step, thereby explaining the depleted Ti and W concentrations in corresponding leachates. However, if this had been the case, one would have also expected similar depletions for other particle reactive elements such as Zr and Hf. Because this is not the case (Fig. 2a), we argue that the observed Ti and W depletions in carbonates simply reflect their very low concentrations in surrounding pore waters at the time of carbonate precipitation, as a consequence of (micro)biogeochemical processes that will be discussed below.

4.2. Trace element enrichments associated with the presence of sulfide minerals

The data obtained on 3M HNO_3 leachates allow us to identify the trace elements that are likely to be preferentially associated with sulfide minerals within seep carbonates. Of course, we are well aware that this leaching step is not selective and may have also led to substantial dissolution of residual carbonate phases, organic compounds and silicate minerals. As a matter of fact, although Ca and Sr in 3M HNO_3 leachates are significantly depleted compared to corresponding carbonate phases (i.e. 1M AA leachates), their presence in 3M HNO_3 leachates clearly indicates that a substantial fraction of the material dissolved by 3M HNO_3 corresponds to carbonates that were left behind the previous 0.25M HCl leaching step. Similarly, a few other trace elements, such as Mn, Ba, REE, W and U, almost systematically display lower concentrations in 3M HNO_3 leachates relative to 1M AA solutions, showing that they are mostly depleted in sulfide minerals. In addition, the pronounced enrichments displayed by elements typically associated with detrital silicates (Ti, Rb, Zr and Th) clearly indicate that partial dissolution of silicate minerals occurred during the leaching step. In contrast, however, the high elemental abundances determined for transition metals (Co, Ni, Cu, Zn, Mo) and Pb in 3M HNO_3 leachates, relative to corresponding carbonate phases, are most likely best explained by the presence of sulfide minerals and/or organic compounds in studied carbonate samples. The relative partitioning of these elements between sulfide and organic phases will be discussed below.

4.3. Trace elements in residual detrital fractions

The residual detrital fractions associated with studied carbonate samples mostly correspond to terrigenous silicate minerals, but also presumably include some refractory organic compounds and/or sulfide minerals that were left behind after the 5% H_2O_2 and 3M HNO_3 leaching steps. In this regard, the most striking feature of the dataset for detrital fractions is the pronounced enrichments in Mo that characterized many samples (Fig. 2c).

In recent years, the distribution of Mo in bulk sediments at cold seeps has received increasing attention, as a potential tracer of methane seepage dynamics (Peketi et al., 2012; Sato et al., 2012; Hu et al., 2015b, Chen et al., 2016). The range of Mo concentrations measured in seep-related sediments from the Nankai Trough (Sato et al., 2012) and the South China Sea (Chen et al., 2016) is similar (up to ~32 mg/kg) to that found in the detrital fractions analyzed in this study (up to 25

mg/kg), being enriched by a factor of about 30 compared to other typical hemipelagic sediments (Sato et al., 2012). This strong Mo enrichment was taken as an evidence that cold seep sediments could possibly represent a net sink in the global biogeochemical marine cycling of Mo (Sato et al., 2012; Hu et al., 2015b). Previous studies have suggested that the enrichment of Mo in marine sediments could relate to high organic contents (Wilde et al., 2004; Guo et al., 2007), or to the presence of high dissolved sulfide (HS^-) concentrations in the sediment, which can lead to conversion of soluble molybdate (MoO_4^{2-}) into particle-reactive thiomolybdate ($MoO_xS_{4-x}^{2-}$) species that are then sequestered within the sediment (Helz et al., 1996; 2011). Clearly, the observed Mo enrichment in the residual silicate fractions associated with seep carbonates can be ascribed to the presence of high dissolved sulfide contents at cold seeps and precipitation of sulfide minerals in the sediment.

Interestingly, we did not identify any particular enrichment for tungsten (W) in studied detrital fractions. Tungsten is the geochemical twin of Mo, and apart from a few differences, both elements generally behave similarly in the marine environment (see Dellwig et al., 2019 for a recent detailed review). In open ocean waters, both Mo and W are intensively scavenged onto Fe-Mn oxyhydroxide phases, which can then be released subsequently into pore waters, following sediment deposition and diagenetic alteration under suboxic/anoxic conditions. Similar to Mo, high sulfide concentrations in pore waters lead to the conversion of tungstate to thiotungstate that can be incorporated into Fe-sulfides or organic compounds. As will be discussed below, the absence of any W enrichment in studied sulfide and detrital fractions, in contrast to Mo, suggests that an unknown mechanism leads to decoupling of Mo and W in cold seep sediments.

4.4. The characteristics of lipid biomarkers and trace elements in organic fractions

The distribution patterns of microbial lipids extracted from our series of authigenic carbonate samples were examined by PCA (Fig. 6). For archaeal lipids, the first PC component (PC1) accounted for 42.0 % of the total variance, and the second PC component (PC2) explained 30.9% of the total variance. The high abundances of isoprenoid DGDs (in particular archaeol and sn-2-hydroxyarchaeol) were responsible for distinguishing between samples for PC1, whereas irregular tail-to-tail isoprenoids (mainly phytane and crocetane) were important for PC2 (Fig. 6a). Based on the PCA results, we also performed a hierarchical clustering of principal components (HCPC) to cluster samples with archaeal lipid abundances. The samples were grouped into three distinct clusters, i.e. Cluster 1, Cluster 2, and Cluster 3 (Fig. 6a). The HCPC results showed that each cluster was associated with distinctive abundances of archaeal lipids investigated. Cluster 3 was associated with the predominant isoprenoid DGDs, which are indicative of AOM-related ANME-1 and -2 assemblages. Cluster 1 with phytane + crocetane is also indicative of ANME-2 related to AOM, but phytane contributions to these samples might be higher than those of Cluster 3. In contrast, Cluster 2 related to PMI, PMI-3, and sn-3-hydroxyarchaeol archaeal lipids are more related to ANME-1 and 2. Among them, the presence of saturated PMI analogue may reflect the growth stages (e.g. lipid biosynthesis) of these communities (Blumenberg et al., 2005; Nauhaus et al., 2007). For bacterial lipids, PC1 and PC2 accounted for 54.4% and 17.3% of the total variance, respectively (Fig. 6b). Most bacterial lipids (i.e. non-isoprenoid DGDs and FAs) were responsible for distinguishing between samples for PC1. The compounds having the strongest influence on PC2 were non-isoprenoid DGDs. Similar to archaeal lipids, bacterial lipids were also grouped into

three distinct clusters (Fig. 6b). Cluster 1 identifies a distinctive group characterized by high DGD (If) contributions. Cluster 2 has also a higher contribution of DGD (If) compared to Cluster 3 characterized, with mixed lipid patterns. In this regard, Cluster 1 and 2 appear to be associated with sulfate reducing bacteria inhabiting cold seep environments (e.g. Pancost et al., 2001).

Compared to leaching with hydrogen peroxide solution, lipid extraction leads to much reduced carbonate dissolution, and hence is probably best suited for investigating organic-bound trace element patterns in seep carbonates. Nevertheless, the two methods result in comparatively similar normalized elemental distribution patterns (Fig. 3), both displaying more or less pronounced enrichments in the following elements: Li, Ti, V, Co, Ni, Cu, Zn, Mo and W. Most of these elements have been already previously identified in microorganism cells, in particular in seep-related microbial assemblages, where they are known to be bound to specific sites of proteins and enzymes (e.g. Barton et al., 2007; Glass and Orphan, 2012). Importantly, this suggests that the determination of trace element patterns in seep carbonates can provide interesting information of the utility of metals to microbial life, and possibly help identifying particular elements with a previously unrecognized importance for microbial metabolism at cold seeps. Microbial metalloenzymes play key roles in catalyzing major biogeochemical reactions, in particular the anaerobic oxidation of methane (Zerkle et al., 2005). The AOM can be largely regarded as a reverse methanogenesis pathway (Hallam et al., 2004; Thauer, 2008; Scheller et al., 2010), and both reactions are thought to require the same combination of trace metals ranging from Fe, Ni, Co, Mo (and/or W) and Zn (Glass and Orphan, 2012). Below, we use our findings on the distribution of trace elements in lipid fractions to further discuss the role of specific metals in microbial methane cycling at cold seeps. In particular, by comparing lipid-bound data with elemental abundances measured in corresponding carbonate and sulfide phases, we can discuss how microbial activity at cold seeps can be affected by trace metal bioavailability in pore waters.

4.4.1. Ni and Co

Both Ni and Co are known to play a crucial role in methanogenesis and anaerobic methanotrophy (e.g. Glass et al., 2012). At submarine methane seeps, Ni-containing proteins were first extracted from microbial mats collected in the Black Sea, which provided one of the first direct evidence for the importance of Ni in the AOM process (Krüger et al., 2003). Various geochemical investigations of methanogenic archaea also revealed significant enrichments of Ni and Co at the cell-scale (Cameron et al., 2012; Glass et al., 2018). A study conducted on Cretaceous methane-derived carbonates identified relatively high Ni signals using laser ablation ICP-MS, which were taken as evidence for past microbial activity (Reitner et al., 2015). To date, at least three Ni-dependent enzymes have been identified in methanogens, including the carbon monoxide dehydrogenase/acetyl-CoA (coenzyme A) synthase, and the Ni cofactor F430 in the methyl coenzyme M reductase, which catalyzes the final step of methanogenesis (Ferry, 1993; Ragsdale and Kumar, 1996). Cobalt is a core element of vitamin B12 (cobalamin) that can be biosynthesized anaerobically by methanogens and sulfate-reducing bacteria, and is involved in methanogenesis and reverse methanogenesis pathways (Glass et al., 2014). In this study, while we did not find any strong relationships between lipid biomarker patterns and elemental concentrations, the abundance of Co in extracted lipid fractions displays positive correlation with C17:0, C18:1w9c and DGD (If). In addition, the slight positive correlations observed between

Ni and Co enrichments in lipid fractions (relative to 3M HNO_3 data) and our PCA results for archaeal lipids (PC1 score; archaeol and *sn*-2-hydroxyarchaeol concentrations) adds further support that measured lipid-bound Ni and Co abundances are related to the presence of archaeal communities (Fig. 7). Importantly, the availability of Ni and Co in natural ecosystems most likely represents a limiting factor for the activity of these archaeal communities (Basiliko and Yavitt, 2001). In this study, the evidence that studied carbonate phases always display relatively high Ni and Co concentrations (Fig. 2) suggests that these elements are generally present in relative abundance in surrounding pore waters. This would indicate that dissolved Ni and Co supply at cold seeps (at least in those investigated during the course of this study) does not represent a limiting factor on microbial activity.

4.4.2. Cu

While the potential utility of Cu in the anaerobic oxidation of methane is yet to be fully understood (Sushkevich et al., 2017), it is well known that Cu plays a central role in the metabolism of aerobic methane-oxidizing bacteria. In presence of Cu, the particulate methane mono-oxygenase (pMMO), a membrane protein found in methanotrophic bacteria, catalyzes the oxidation of methane to methanol. An increase in Cu concentration can result in up to 55-fold expression of pMMO (Glass and Orphan, 2012). In this study, while lipid-bound Cu concentrations in seep carbonates do not appear to correlate with lipid biomarker patterns, a few aragonite-rich seep carbonates (sample 2-3, 2-4, with Sr/Ca > 0.020) appear to host microbial lipid fractions characterized by higher Cu contents (as inferred from Cu/Ca ratios; Fig. 5). As already mentioned above, aragonite precipitation at cold seeps is favored at sites characterized by high methane fluxes, where the SMTZ is located at shallower sediment depth, in the near-seafloor environment (e.g., Burton, 1993; Bayon et al, 2007; Peckmann et al, 2009; Nöthen and Kasten, 2011). Near the sediment-water interface, it is likely that methane oxidation partly proceeds through Cu-dependent aerobic methane-oxidizing bacteria, which would possibly explain why lipid fractions extracted from a few aragonite-rich carbonates display higher Cu contents than those recovered from high-Mg carbonate phases (which presumably formed from deeper and fully anoxic sediment layers). This would be in full agreement with previous biomarker investigations, which also identified the presence of aerobic methanotrophs in seep carbonates formed near the seafloor (Himmler et al., 2015).

4.4.3. Mo and W

Molybdenum (Mo) and its geochemical twin tungsten (W) are also important metals in the metabolism of microbial communities involved in the AOM, especially when it is coupled to nitrate reduction (Haroon et al., 2013; Glass et al., 2014). The most well-known biological function for Mo is as nitrate reductase and nitrogenase enzyme (Kisker et al., 1997; Zerkle et al., 2005; Glass and Orphan, 2012; Mcglynn et al., 2013), in which Mo (or W) is bound to a pterin cofactor to form molybdopterin (or tungstopterin). Some methanogens also require Mo and/or W in formyl-methanofuran dehydrogenases system, which catalyze the initial conversion of carbon dioxide to methane (L'vov et al., 2002; Ferry, 2010).

In this study, Mo and W were found to be significantly enriched in lipid fractions, although no major correlation could be identified between lipid-bound Mo-W trace element data and our PCA

results for archaeal lipids (figure not shown here). The ubiquitous presence of Mo in all studied fractions, including lipids but also corresponding carbonate and sulfide mineral phases, indicates the abundance of bioavailable Mo at cold seeps. In contrast, while W also display pronounced enrichments in lipid-bound fractions, the low W concentrations determined in both carbonate phases and sulfide minerals at seeps suggest instead that dissolved W concentrations in surrounding pore waters are relatively depleted. While this assumption agrees with a previous trace metal investigation of pore waters at Hydrate Ridge (Glass et al., 2014), which reported very low dissolved W concentrations at methane seeps, it is in contrast with the fact that thiotungstate should be more soluble than thiomolybdate species in pore waters (Mohajerin et al., 2014; 2016). Based on the above, we speculate that the low W abundances in seep carbonate and sulfide phases (and presumably in pore waters) reflect substantial microbial requirements in W during the AOM. This hypothesis would be supported by previous evidence of striking correlations between W enrichments and the presence of hyperthermophiles in hydrothermal mineral deposits (Holden and Adams, 2003), suggesting that W may be preferred over Mo by anaerobic microbial communities at submarine methane seeps (L'vov et al., 2002; Holden and Adams, 2003).

5. Conclusions

Our combined investigation of trace element systematics in authigenic carbonates and associated lipid fractions provides evidence for the utility of trace metals to microbial life at cold seeps. While trace element distribution patterns of inorganic carbonate phases mainly reflect the chemical composition of surrounding pore waters at the time of carbonate precipitation, pronounced trace metal enrichments associated with total lipid fractions for Ni, Co, Cu, Mo and W relate to their implication in various microbial enzymatic activities.

The abundance of Ni, Co and Mo is ubiquitous in studied lipid biomarkers, but also in corresponding carbonate phases and sulfide minerals, suggesting that a substantial pool of dissolved Ni, Co and Mo is available at cold seeps for the microorganisms involved in the anaerobic oxidation of methane. In contrast, we propose that important microbial requirement in W during the AOM can lead to strong depletion of dissolved W in pore waters at cold seeps, as inferred from the very low W concentrations determined in both carbonate phases and sulfide minerals. This finding suggests that W could represent a limiting factor for microbial methane oxidation at seeps. Overall, this study demonstrates the utility of combining trace element systematics to lipid biomarker investigations in order to improve our understanding of the microbial biogeochemistry of deep-sea extreme environments.

Acknowledgments

This project was funded by IFREMER; the National Research Foundation of Korea (NRF) grants funded by the Ministry of Science and ICT (MSIT) – South Korea [NRF-2016R1A2B3015388, KOPRI-PN19100 and NRF-2015M1A5A1037243, KOPRI-PN19090]; and the National Key R&D Program of China (2018YFC0310003), the National Program on Global Change and Air-Sea Interaction (GASI-GEOGE-05-04), and the NSF of China (Grants: 41773091, 41730528, and 41761134084). We thank H.H. Roberts for providing the Gulf of Mexico seep carbonate samples.

Xudong Wang acknowledges the China Scholarship Council for supporting a research visit to IFREMER.

References

Aloisi, G., Pierre, C., Rouchy, J.M., Foucher, J.P., Woodside, J., the MEDINAUT Scientific Party, 2000. Methane-related authigenic carbonates of eastern Mediterranean Sea mud volcanoes and their possible relation to gas hydrate destabilisation. Earth Planet. Sci. Lett. 184, 321–338.

Aloisi, G., Bouloubassi, I., Heijs, S.K.,Pancost, R.D., Pierre, C., Sinninghe Damsté, J.P., Gottschal, J.C., Forney, L.J., Rouchy, J-M., 2002. CH_4-consuming microorganisms and the formation of carbonate crusts at cold seeps. Earth Planet. Sci. Lett. 203, 195-203.

Anbar, A.D., 2008. Elements and Evolution. Science 322, 1481–1483.

Barrat, J.A., Keller, F., Amossé. J., Taylor, R.N., Nesbitt, R.W., Hirata, T., 1996. Determination of rare earth elements in sixteen silicate reference samples by ICP-MS after Tm addition and ion-exchange separation. Geostand. Geoanal. Res. 20, 133–139.

Barrat, J.A., Zanda, B., Moynier, F., Bollinger, C., Liorzou, C., Bayon, G., 2012. Geochemistry of CI chondrites: Major and trace elements, and Cu and Zn Isotopes. Geochim. Cosmochim. Acta 83, 79–92.

Barton, L.L., Goulhen, F., Bruschi, M., Woodards, N.A., Plunkett, R.M., Rietmeijer, F.J.M., 2007. The bacterial metallome: composition and stability with specific reference to the anaerobic bacteriumDesulfovibrio desulfuricans. Biometals 20, 291–302.

Basiliko, N., Yavitt, J.B., 2001. Influence of Ni, Co, Fe, and Na additions on methane production in Sphagnum-dominated Northern American peatlands. Biogeochemistry 52, 133–153.

Bayon, G., German, C.R., Boella, R.M., Milton, J.A., Taylor, R.N., Nesbitt, R.W, 2002. An improved method for extracting marine sediment fractions and its application to Sr and Nd isotopic analysis. Chem. Geol. 187, 179–199.

Bayon, G., Pierre, C., Etoubleau, J., Voisset, M., Cauquil, E., Marsset, T., Sultan, N., Le Drezen, E., Fouquet, Y., 2007. Sr/Ca and Mg/Ca ratios in Niger Delta sediments: implications for authigenic carbonate genesis in cold seep environments. Mar. Geol. 241, 93–109.

Bayon, G., Barrat, J.A., Etoubleau, J., Benoit, M., Bollinger, C., Révillon, S., 2009. Determination of rare earth elements, Sc, Y, Zr, Ba, Hf and Th in geological samples by ICP-MS after Tm addition and alkaline fusion. Geostand. Geoanal. Res. 33, 51–62.

Bayon, G., Birot, D., Ruffine, L., Caprais, J.-C., Ponzevera, E., Bollinger, C., Donval, J.-P., Charlou, J.-L., Voisset, M., Grimaud, S., 2011a. Evidence for intense REE scavenging at cold

691 seeps from the Niger Delta margin. Earth Planet. Sci. Lett. 312, 443–452.
692
693 Bayon, G., Birot, D., Bollinger, C., Barrat, J-A., 2011b. Multi-Element Determination of Trace
694 Elements in Natural Water Reference Materials by ICP-SFMS after Tm Addition and Iron
695 Co-precipitation. Geostand. Geoanal. Res. 35, 145–153.
696
697 Bayon, G., Toucanne, S., Skonieczny, C., André, L., Bermell, S., Cheron, S., Dennielou, B.,
698 Etoubleau, J., Freslon, N., Gauchery, T., Germain, Y., Jorry, S.J., Ménot, G., Monin, L., Ponzevera,
699 E., Rouget, M.-L., Tachikawa, K., Barrat, J.A., 2015. Rare earth elements and neodymium
700 isotopes in world river sediments revisited. Geochim. Cosmochim. Acta 170, 17–38.
701
702 Beal, E.J., House, C.H., Orphan, V.J., 2009. Manganese- and Iron-Dependent Marine Methane
703 Oxidation. Science 325, 184–187.
704
705 Blumenberg, M., Seifert, R., Nauhaus, K., Pape, T., Michaelis, W., 2005. In Vitro Study of Lipid
706 Biosynthesis in an Anaerobically Methane-Oxidizing Microbial Mat. Appl. Environ. Microbiol. 71,
707 4345–4351.
708
709 Boetius, A., Ravenschlag, K., Schubert, C.J., Rickert, D., Widdel, F., Gieseke, A., Amann, R.,
710 Jørgensen, B.B., Witte, U., Pfannkuche, O., 2000. A marine microbial consortium apparently
711 mediating anaerobic oxidation of methane. Nature 407, 623–626.
712
713 Burton, E.A., 1993. Controls on marine carbonate cement mineralogy: review and reassessment.
714 Chem. Geol. 105, 163–179.
715
716 Cameron, V., House, C.H., Brantley, S.L., 2012. A First Analysis of Metallome Biosignatures of
717 Hyperthermophilic Archaea. Archaea, 1–12.
718
719 Cangemi, M., Leonardo, R.D., Bellanca, A., Cundy, A., Neri, R., Angelone, M., 2010.
720 Geochemistry and mineralogy of sediments and authigenic carbonates from the Malta Plateau,
721 Strait of Sicily (Central Mediterranean): Relationships with mud/fluid release from a mud volcano
722 system. Chem. Geol. 276, 294–308.
723
724 Chao, T.T., Sanzolone, R.F., 1977. Chemical dissolution of sulfide minerals. Journal of Research
725 of the U.S. Geological Survey 5, 409–412.
726
727 Chen, F., Hu, Y., Feng, D., Zhang, X., Cheng, S., Cao, J., Lu, H., Chen D., 2016. Evidence of
728 intense methane seepages from molybdenum enrichments in gas hydrate-bearing sediments of the
729 northern South China Sea. Chem. Geol. 443, 173–181.
730
731 Conti, S., Fontana, D., Gubertini, A., Sighinolfi, G., Tateo, F., Fioroni, C., Fregni, P., 2004. A
732 multidisciplinary study of middle Miocene seep-carbonates from the northern Apennine foredeep
733 (Italy). Sediment. Geol. 169, 1–19.
734

Dellwig, O., Wegwerth, A., Schnetger, B., Schulz, H., Arz, H.W., 2019. Dissimilar behaviors of the geochemical twins W and Mo in hypoxic-euxinic marine basins. Earth-Sci. Rev. 193, 1–23.

Dold, B., 2003. Speciation of the most soluble phases in a sequential extraction procedure adapted for geochemical studies of copper sulfide mine waste. J. Geochem. Explor. 80, 55–68.

Feng, D., Chen, D., Peckmann, J., 2009. Rare earth elements in seep carbonates as tracers of variable redox conditions at ancient hydrocarbon seeps. Terr. Nova 21, 49–56.

Feng, D., Roberts, H.H., 2010. Initial results of comparing cold-seep carbonates from mussel- and tubeworm-associated environments at Atwater Valley lease block 340, northern Gulf of Mexico. Deep-Sea Res. Part II-Top. Stud. Oceanogr. 57, 2030–2039.

Feng, D., Roberts, H.H., 2011. Geochemical characteristics of the barite deposits at cold seeps from the northern Gulf of Mexico continental slope. Earth Planet. Sci. Lett. 309, 89–99.

Feng, D., Chen, D., 2015. Authigenic carbonates from an active cold seep of the northern South China Sea: new insights into fluid sources and past seepage activity. Deep-Sea Res. Part II-Top. Stud. Oceanogr. 122, 74–83.

Ferry, J.G., 1993. Methanogenesis: Ecology, Physiology, Biochemistry & Genetics, Chapman & Hall, New York, NY, USA.

Ferry, J.G., 2010. How to make a living by exhaling methane. Annu. Rev. Microbiol. 64, 453–473.

Freslon, N., Bayon, G., Birot, D., Bollinger, C., Barrat, J.A., 2011. Determination of rare earth elements and other trace elements (Y, Mn, Co, Cr) in seawater using Tm addition and $Mg(OH)_2$ co-precipitation. Talanta 85, 582–587.

Freslon, N., Bayon, G., Toucanne, S., Bermell, S., Bollinger, C., Chéron, S., Etoubleau, J., Germain, Y., Khripounoff, A., Ponzevera, E., Rouget, M.L., 2014. Rare earth elements and neodymium isotopes in sedimentary organic matter. Geochim. Cosmochim. Acta 140, 177–198.

Frimmel, H.E., 2009. Trace element distribution in Neoproterozoic carbonates as palaeoenvironmental indicator. Chem. Geol. 258, 338–353.

Ge, L., Jiang, S., Swennen, R., Yang, T., Yang, J., Wu, N., Liu, J., Chen D., 2010. Chemical environment of cold seep carbonate formation on the northern continental slope of South China Sea: Evidence from trace and rare earth element geochemistry. Mar. Geol. 277, 21–30.

Ge, L., Jiang, S., 2013. Sr isotopic compositions of cold seep carbonates from the South China Sea and the Panoche Hills (California, USA) and their significance in palaeooceanography. J. Asian Earth Sci. 65, 34–41.

779 Glass, J.B., Orphan, V.J., 2012. Trace Metal Requirements for Microbial Enzymes Involved in the
780 Production and Consumption of Methane and Nitrous Oxide. Front. Microbiol. 3, 61.
781 doi:10.3389/fmicb.2012.00061.
782
783 Glass, J.B., Yu, H., Steele, J.A., Dawson, K.S., Sun, S., Chourey, K., Pan, C., Hettich, R.L.,
784 Orphan, V.J., 2014. Geochemical, metagenomic and metaproteomic insights into trace metal
785 utilization by methane-oxidizing microbial consortia in sulphidic marine sediments. Environ.
786 Microbiol. 16, 1592–1611.
787
788 Glass, J.B., Chen, S., Dawson, K.S., Horton, D.R., Vogt, S., Ingall, E.D., Twining, B.S., Orphan,
789 V.J., 2018. Trace Metal Imaging of Sulfate-Reducing Bacteria and Methanogenic Archaea at
790 Single-Cell Resolution by Synchrotron X-Ray Fluorescence Imaging. Geomicrobiol. J. 1-9, doi:
791 10.1080/01490451.2017.1321068.
792
793 Guan, H., Feng, D., Wu, N., Chen, D., 2016. Methane seepage intensities traced by biomarker
794 patterns in authigenic carbonates from the South China Sea. Org. Geochem. 91, 109–119.
795
796 Guo, Q., Shields, G.A., Liu, C., Strauss, H., Zhu, M., Pi, D., Goldberg, T., Yang, X., 2007. Trace
797 element chemostratigraphy of two Ediacaran–Cambrian successions in south China: Implications
798 for organosedimentary metal enrichment and silicification in the Early Cambrian. Palaeogeogr.
799 Palaeoclimatol. Palaeoecol. 254, 194–216.
800
801 Haley, B.A., Klinkhammer, G.P., Mcmanus, J., 2004. Rare earth elements in pore waters of marine
802 sediments. Geochim. Cosmochim. Acta 68, 1265–1279.
803
804 Hallam, S.J., Putman, N., Preston, C.M., Detter, J.C., Rokhsar, D., Richardson, P.M., DeLong, E.F.,
805 2004. Reverse methanogenesis: testing the hypothesis with environmental genomics. Science 305,
806 1457–1462.
807
808 Haroon, M.F., Hu, S., Shi, Y., Imelfort, M., Keller, J., Hugenholtz, P., Yuan, Z., Tyson, G.W., 2013.
809 Anaerobic oxidation of methane coupled to nitrate reduction in a novel archaeal lineage. Nature
810 500, 567–570.
811
812 Helz, G.R., Miller, C.V., Charnock, J.M., Mosselmans, J.F.W., Pattrick, R.A.D., Garner, C.D.,
813 Vaughan, D.J., 1996. Mechanism of molybdenum removal from the sea and its concentration in
814 black shales: EXAFS evidence. Geochim. Cosmochim. Acta 60, 3631–3642.
815
816 Helz, G.R., Bura-Nakić, E., Mikac, N., Ciglenečki, I., 2011. New model for molybdenum behavior
817 in euxinic waters. Chem. Geol. 284, 323–332.
818
819 Himmler, T., Bach, W., Bohrmann, G., Peckmann, J., 2010. Rare earth elements in authigenic
820 methane-seep carbonates as tracers for fluid composition during early diagenesis. Chem. Geol.
821 277, 126–136.
822

Himmler, T., Birgel, D., Bayon, G., Pape, T., Ge, L., Bohrmann, G., Peckmann, J., 2015. Formation of seep carbonates along the Makran convergent margin, northern Arabian Sea and a molecular and isotopic approach to constrain the carbon isotopic composition of parent methane. Chem. Geol. 415, 102–117.

Holden, J.F., Adams, M.W.W., 2003. Microbe-metal interactions in marine hydrothermal environments. Curr. Opin. Chem. Biol. 7, 160–165.

Hu, Y., Feng, D., Peckmann, J., Roberts, H.H., Chen, D., 2014. New insights into cerium anomalies and mechanisms of trace metal enrichment in authigenic carbonate from hydrocarbon seeps. Chem. Geol. 381, 55–66.

Hu, Y., Feng, D., Chen, L., Zheng, G., Peckmann, J., Chen, D., 2015a. Using iron speciation in authigenic carbonates from hydrocarbon seeps to trace variable redox conditions. Mar. Pet. Geol. 67, 111–119.

Hu, Y., Feng, D., Liang, Q., Xia, Z., Chen, L., Chen, D., 2015b. Impact of anaerobic oxidation of methane on the geochemical cycle of redox-sensitive elements at cold-seep sites of the northern South China Sea. Deep-Sea Res. Part II-Top. Stud. Oceanogr. 122, 84–94.

Jahn, B., Pol, A., Lumpe, H., Barends, T.R.M., Dietl, A., Hogendoorn, C., Op den Camp, H.J.M., Daumann, L.J., 2018. Similar but Not the Same: First Kinetic and Structural Analyses of a Methanol Dehydrogenase Containing a Europium Ion in the Active Site. ChemBioChem, doi: 10.1002/cbic.201800130.

Jochum, K.P., Weis, U., Schwager, B., Stoll, B., Wilson, S.A., Haug, G.H., Andreae, M.O., Enzweiler, J., 2016. Reference Values Following ISO Guidelines for Frequently Requested Rock Reference Materials. Geostand. Geoanal. Res. 40, 333–350.

Jørgensen, N.O., 1992. Methane-derived carbonate cementation of marine sediments from the Kattegat, Denmark: Geochemical and geological evidence. Mar. Geol. 103, 1–13.

Joye, S.B., Boetius, A., Orcutt, B.N., Montoya, J.P., Schulz, H.N., Erickson, M.J., Lugo, S.K., 2004. The anaerobic oxidation of methane and sulfate reduction in sediments from Gulf of Mexico cold seeps. Chem. Geol. 205, 219–238.

Kisker, C., Schindelin, H., Rees, D.C., 1997. Molybdenum-cofactor-containing enzymes: structure and mechanism. Annu. Rev. Biochem. 66, 233–267.

Konhauser, K.O., Pecoits, E., Lalonde, S.V., Papineau, D., Nisbet, E.G., Barley, M.E., Arndt, N.T., Zahnle, K., Kamber, B.S., 2009. Oceanic nickel depletion and a methanogen famine before the great oxidation event. Nature 458, 750–753.

Krüger, M., Meyerdierks, A., Glockner, F.O., Amann, R., Widdel, F., Kube, M., Reinhardt, R.,

Kahnt, J., Böcher, R., Thauer, R.K., Shima, S., 2003. A conspicuous nickel protein in microbial mats that oxidize methane anaerobically. Nature 426, 878–881

Lee, D.H., Kim, J.H., Lee, Y.M., Stadnitskaia, A., Jin, Y.K., Niemann, H., Kim, Y.G., Shin, K.H., 2018. Biogeochemical evidence of anaerobic methane oxidation on active submarine mud volcanoes on the continental slope of the Canadian Beaufort Sea. Biogeosciences, 15, 7419–7433.

Lemaitre, N., Bayon, G., Ondréas, H., Caprais, J.C., Freslon, N., Bollinger, C., Rouget, M.L., de Prunelé, A., Ruffine, L., Roy, K.O.L., Sarthou, G., 2014. Trace element behaviour at cold seeps and the potential export of dissolved iron to the ocean. Earth Planet. Sci. Lett. 404, 376–388.

Levin, L.A., 2005. Ecology of cold seep sediments: Interactions of fauna with flow, chemistry and microbes. Oceanogr. Mar. Biol. 43, 1–46.

Liang, Q., Hu, Y., Feng, D., Peckmann, J., Chen, L., Yang, S., Liang, J., Tao, J., Chen, D., 2017. Authigenic carbonates from newly discovered active cold seeps on the northwestern slope of the South China Sea: Constraints on fluid sources, formation environments, and seepage dynamics. Deep-Sea Res. Part I-Oceanogr. Res. Pap. 124, 31–41.

Lu, Y., Liu, Y., Sun, X., Lin, Z., Xu, L., Lu, H., Hao, X., Peckmann, J., 2017. Intensity of methane seepage reflected by relative enrichment of heavy magnesium isotopes in authigenic carbonates: A case study from the South China Sea. Deep-Sea Res. Part I-Oceanogr. Res. Pap. 129, 10–21.

Luff, R., Wallmann, K., 2003. Fluid flow, methane fluxes, carbonate precipitation and biogeochemical turnover in gas hydrate-bearing sediments at Hydrate Ridge, Cascadia Margin: numerical modeling and mass balances. Geochim. Cosmochim. Acta 67, 3403–3421.

L'vov, N. P., Nosikov, A. N., Antipov, A. N., 2002. Tungsten-containing enzymes. Biochem.-Moscow 67, 196–200.

Mcglynn, S.E., Boyd, E.S., Peters, J.W., Orphan, V.J., 2013. Classifying the metal dependence of uncharacterized nitrogenases. Front. Microbiol. 3, 1–8.

Michaelis, W., Seifert, R., Nauhaus, K., Treude, T., Thiel, V., Blumenberg, M., Knittel, K., Gieseke, A., Peterknecht, K., Pape, T., Boetius, A., Amann, R., Jørgensen, B.B., Widdel, F., Peckmann, J., Pimenov, N.V., Gulin, M.B. 2002. Microbial Reefs in the Black Sea Fueled by Anaerobic Oxidation of Methane. Science 297, 1013–1015.

Mohajerin, T.J., Helz, G.R., White, C.D., Johannesson, K.H., 2014. Tungsten speciation in sulfidic waters: Determination of thiotungstate formation constants and modeling their distribution in natural waters. Geochim. Cosmochim. Acta 144:157–172.

Mohajerin, T.J., Helz, G.R., Johannesson, K.H., 2016. Tungsten–molybdenum fractionation in estuarine environments. Geochim. Cosmochim. Acta 177, 105–119.

Morford, J.L., Emerson, S., 1999. The geochemistry of redox sensitive trace metals in sediments. Geochim. Cosmochim. Acta 63, 1735–1750.

Nance, W.B., Taylor, S.R., 1976. Rare earth element patterns and crustal evolution—I. Australian post-Archean sedimentary rocks. Geochim. Cosmochim. Acta 40, 1539–1551.

Nauhaus, K., Albrecht, M., Elvert, M., Boetius, A., Widdel, F., 2007. In vitro cell growth of marine archaeal-bacterial consortia during anaerobic oxidation of methane with sulfate. Environ. Microbiol. 9, 187–196.

Nothdurft, L.D., Webb, G.E., Kamber, B.S., 2004. Rare earth element geochemistry of Late Devonian reefal carbonates, Canning Basin, western Australia: confirmation of a seawater REE proxy in ancient limestones. Geochim. Cosmochim. Acta 68, 263–283.

Nöthen, K., Kasten, S., 2011. Reconstructing changes in seep activity by means of pore water and solid phase Sr/Ca and Mg/Ca ratios in pockmark sediments of the northern Congo Fan. Mar. Geol. 287, 1–13.

Pancost, R.D., Bouloubassi, I., Aloisi, G., Damsté, J.S.S., the Medinaut Shipboard Scientific Party, 2001. Three series of non-isoprenoidal dialkyl glycerol diethers in cold-seep carbonate crusts. Org. Geochem. 32, 695–707

Peckmann, J., Reimer, A., Luth, U., Luth, C., Hansen, B., Heinicke, C., Hoefs, J., Reitner, J., 2001. Methane-derived carbonates and authigenic pyrite from the northwestern Black Sea. Mar. Geol. 177, 129–150.

Peckmann, J., Birgel, D., Kiel, S., 2009. Molecular fossils reveal fluid composition and flow intensity at a Cretaceous seep. Geology 37, 847–850.

Peketi, A., Mazumdar, A., Joshi, R.K., Patil, D.J., Srinivas, P.L., Dayal, A.M., 2012. Tracing the Paleo sulfate-methane transition zones and H2S seepage events in marine sediments: An application of C-S-Mo systematics. Geochem. Geophys. Geosyst. 13, Q10007, doi:10.1029/2012GC004288.

Picone, N., Op den Camp, H.J.M., 2019. Role of rare earth elements in methanol oxidation. Curr. Opin. Chem. Biol. 49, 39–44.

Pierre, C., Fouquet, Y., 2007. Authigenic carbonates from methane seeps of the Congo deep-sea fan. Geo-Mar. Lett. 27, 249–257.

Pingitore Jr, N.E., Eastman, M.P., 1984. The experimental partitioning of Ba^{2+} into calcite. Chem. Geol. 45, 113–120.

Pol, A., Barends, T.R.M., Dietl, A., Khadem, A.F., Eygensteyn, J., Jetten, M.S.M., Op den Camp, H.J.M., 2014. Rare earth metals are essential for methanotrophic life in volcanic mudpots. Environ. Microbiol. 16, 255–264.

Raghoebarsing, A.A., Pol, A., van de P-S, K.T., Smolders, A.J.P., Ettwig, K.F., Rijpstra, W.I.C., Schouten, S., Sinninghe Damsté, J.S., Op den Camp, H.J.M., Jetten, M.S.M., Strous, M., 2006. A microbial consortium couples anaerobic methane oxidation to denitrification. Nature 440, 918–921.

Ragsdale, S.W., Kumar, M., 1996. Nickel-Containing Carbon Monoxide Dehydrogenase/Acetyl-CoA Synthase. Chem. Rev. 96(7), 2515–2540.

Reinhard, C.T., Lalonde, S.V., Lyons, T.W., 2013. Oxidative sulfide dissolution on the early Earth. Chem. Geol. 362, 44–55.

Reitner, J., Blumenberg, M., Walliser, E.O., Schäfer, N., Duda, J.P., 2015. Methane-derived carbonate conduits from the late Aptian of Salinac (Marne Bleues, Vocontian Basin, France): Petrology and biosignatures. Mar. Pet. Geol. 66, 641–652.

Roberts, H.H., Feng, D., Joye, S.B., 2010. Cold-seep carbonates of the middle and lower continental slope, northern Gulf of Mexico. Deep-Sea Res. Part II-Top. Stud. Oceanogr. 57, 2040–2054.

Rongemaille, E., Bayon, G., Pierre, C., Bollinger, C., Chu, N.C., Fouquet, Y., Riboulot, V., Voisset, M., 2011. Rare earth elements in cold seep carbonates from the Niger delta. Chem. Geol. 286, 196–206.

Sarkar, A., Sarangi, S., Ebihara, M., Bhattacharya, S.K., Ray, A.K., 2003. Carbonate geochemistry across the Eocene/Oligocene boundary of Kutch, western India: implications to oceanic O2-poor condition and foraminiferal extinction. Chem. Geol. 201, 281–293.

Sato, H., Hayashi, K.I., Ogawa, Y., Kawamura, K., 2012. Geochemistry of deep sea sediments at cold seep sites in the Nankai Trough: Insights into the effect of anaerobic oxidation of methane. Mar. Geol. 323–325.

Savard, M.M., Beauchamp, B., Veizer, J., 1996. Significance of Aragonite Cements Around Cretaceous Marine Methane Seeps. J. Sediment. Res. 66(3), 430–438.

Scheller, S., Goenrich, M., Boecher, R., Thauer, R.K., Jaun, B., 2010. The key nickel enzyme of methanogenesis catalyses the anaerobic oxidation of methane. Nature 465, 606–608.

Scheller, S., Ermler, U., Shima, S., 2017. Catabolic Pathways and Enzymes Involved in Anaerobic Methane Oxidation. Anaerobic Utilization of Hydrocarbons, Oils, and Lipids, Handbook of Hydrocarbon and Lipid Microbiology, doi:10.1007/978-3-319-33598-8_3-1.

Scherer, P., Lippert, H., Wolff, G., 1983. Composition of the major elements and trace elements of 10 methanogenic bacteria determined by inductively coupled plasma emission spectrometry. Biol. Trace Elem. Res. 5, 149–163.

Sibuet, M., Olu, K., 1998. Biogeography, biodiversity and fluid dependence of deep-sea cold-seep communities at active and passive margins. Deep-Sea Res. Part II-Top. Stud. Oceanogr. 45, 517–567.

Snyder, G.T., Hiruta, A., Matsumoto, R., Dickens, G.R., Tomaru, H., Takeuchi, R., Komatsubara, J., Ishida, Y., Yu, H., 2007. Pore water profiles and authigenic mineralization in shallow marine sediments above the methane-charged system on Umitaka Spur, Japan Sea. Deep-Sea Res. Part II-Top. Stud. Oceanogr. 54, 1216–1239.

Soyol-Erdene, T.-O., Huh, Y., 2013. Rare earth element cycling in the pore waters of the Bering Sea Slope (IODP Exp. 323). Chem. Geol. 358, 75–89.

Stadnitskaia, A., Ivanov, M.K., Damsté, J.S.S., 2008. Application of lipid biomarkers to detect sources of organic matter in mud volcano deposits and post-eruptional methanotrophic processes in the Gulf of Cadiz, NE Atlantic. Mar. Geol. 255, 1–14.

Straaten, F.V.D., Schenk, V., John, T., Gao, J., 2008. Blueschist-facies rehydration of eclogites (Tian Shan, NW-China): Implications for fluid–rock interaction in the subduction channel. Chem. Geol. 255, 195–219.

Sun, Z., Wei, H., Zhang, X., Shang, L., Yin, X., Sun, Y., Xu, L., Huang, W., Zhang, X., 2015. A unique Fe-rich carbonate chimney associated with cold seeps in the Northern Okinawa Trough, East China Sea. Deep-Sea Res. Part I-Oceanogr. Res. Pap. 95, 37–53.

Sushkevich, V.L., Palagin, D., Ranocchiari, M., Bokhoven J.A.van., 2017. Selective anaerobic oxidation of methane enables direct synthesis of methanol. Science 356, 523–527.

Tachikawa, K., Piotrowski, A.M., Bayon, G., 2014. Neodymium associated with foraminiferal carbonate as a recorder of seawater isotopic signatures. Quat. Sci. Rev. 88,1–13.

Taylor, S.R., McLennan, S.M., 1985. The Continental Crust: Its Composition and Evolution. An Examination of the Geochemical Record Preserved in Sedimentary Rocks. Blackwell Scientific Publications, Oxford.

Thauer, R.K., Shima, S., 2008. Methane as fuel for anaerobic microorganisms. Ann. NY Acad. Sci. 1125, 158–170.

Thauer, R.K., Kaster, A.K., Goenrich, M., Schick, M., Hiromoto, T., Shima, S., 2010. Hydrogenases from Methanogenic Archaea, Nickel, a Novel Cofactor, and H2 Storage. Annu. Rev.

Biochem. 79, 507–536.

Torres, M.E., Mcmanus, J., Huh, C.A., 2002. Fluid seepage along the San Clemente Fault scarp: basin-wide impact on barium cycling. Earth Planet. Sci. Lett. 203, 181–194.

Torres, M.E., Martin, R.A., Klinkhammer, G.P., Nesbitt, E.A., 2010. Post depositional alteration of foraminiferal shells in cold seep settings: New insights from flow-through time-resolved analyses of biogenic and inorganic seep carbonates. Earth Planet. Sci. Lett. 299, 10–22.

Tribovillard, N., Du Châtelet, E.A., Gay, A., Barbecot, F., Sansjofre, P., Potdevin, J.L., 2013. Geochemistry of cold seepage-impacted sediments: Per-ascensum or per-descensum trace metal enrichment? Chem. Geol. 340, 1–12.

Vigneron, A., Cruaud, P., Pignet, P., Caprais, J.C., Cambon-Bonavita, M.A., Godfroy, A., Toffin L., 2013. Archaeal and anaerobic methane oxidizer communities in the Sonora Margin cold seeps, Guaymas Basin (Gulf of California). The ISME Journal 7,1595–1608.

Wang, Q., Chen, D., Peckmann, J., 2019. Iron shuttle controls on molybdenum, arsenic, and antimony enrichment in Pliocene methane-seep carbonates from the southern Western Foothills, Southwestern Taiwan. Mar. Pet. Geol. 100, 263–269.

Wilde, P., Lyons, T.W., Quinby-Hunt, M.S., 2004. Organic carbon proxies in black shales: molybdenum. Chem. Geol. 206, 167–176.

Yunker, M.B., Belicka, L.L., Harvey, H.R., Macdonald, R.W., 2005. Tracing the inputs and fate of marine and terrigenous organic matter in Arctic Ocean sediments: A multivariate analysis of lipid biomarkers. Deep-Sea Res. Part II-Top. Stud. Oceanogr. 52, 3478–3508.

Zerkle, A.L., House, C.H., Brantley, S.L., 2005. Biogeochemical signatures through time as inferred from whole microbial genomes. Am. J. Sci. 305, 467–502.

Figure captions

Figure 1. Global map showing the five study areas: 1) Congo fan; 2) Nile deep-sea fan; 3) Niger fan; 4) Eastern Mediterranean Sea; 5) Gulf of Mexico.

Figure 2. Enrichment factor of inorganic fractions (carbonate phases + sulfide minerals + detrital silicate fractions). (a) 1M acetic acid (AA) leachate data normalized to values for the JLs-1 carbonate reference material; (b) 3M HNO_3 leachate data normalized to values for corresponding 1M AA leachates; (c) conc. HF + HCl data normalized to post-Archaean Australian shale (PAAS) reference values.

Figure 3. Enrichment factor of organic fractions (organic compounds + lipid biomarkers). (a) 5% H_2O_2 leachate data normalized to values for corresponding 1M acetic acid (AA) leachates; (b) 5%

H_2O_2 leachate data normalized to values for corresponding 3M HNO_3 leachates; (c) lipid-bound trace element data normalized to values for 1M AA leachates; (d) lipid-bound trace-element data normalized to values for 3M HNO_3 leachates.

Figure 4. Metal/Ca ratios in 1M acetic acid (AA) leachates. (a) Sr/Ca versus Mn/Ca; (b) Sr/Ca versus U/Ca; (c) Sr/Ca versus Ba/Ca; (d) Sr/Ca versus Nd/Ca.

Figure 5. Cu/Ca ratios in extracted lipid fractions versus Sr/Ca in corresponding 1M acetic acid (AA) leachates.

Figure 6. Principal component analysis (PCA) results for microbial lipid biomarkers. (a) archaeal and (b) bacterial compounds.

Figure 7. Results of PCA for archaeal lipids (PC1 score) versus enrichment factors for Ni and Co in carbonate-hosted lipid fractions. The slight positive correlations provide support that lipid-bound Ni and Co abundances are related to archaeal and *sn*-2-hydroxyarchaeal concentrations.

Table captions

Table 1. Site information, water depth, mineral compositions, and carbon and oxygen stable isotopic data for the seep carbonate analyzed in this study.

Table 2. Trace element abundances (mg/kg) of certified reference materials (BHVO-2 and JLs-1).

Table 3. Element concentrations (mg/kg) of studied cold seep carbonate samples.

Table 4. Concentrations of archaeal and bacterial lipids.


4
2
5
3
1

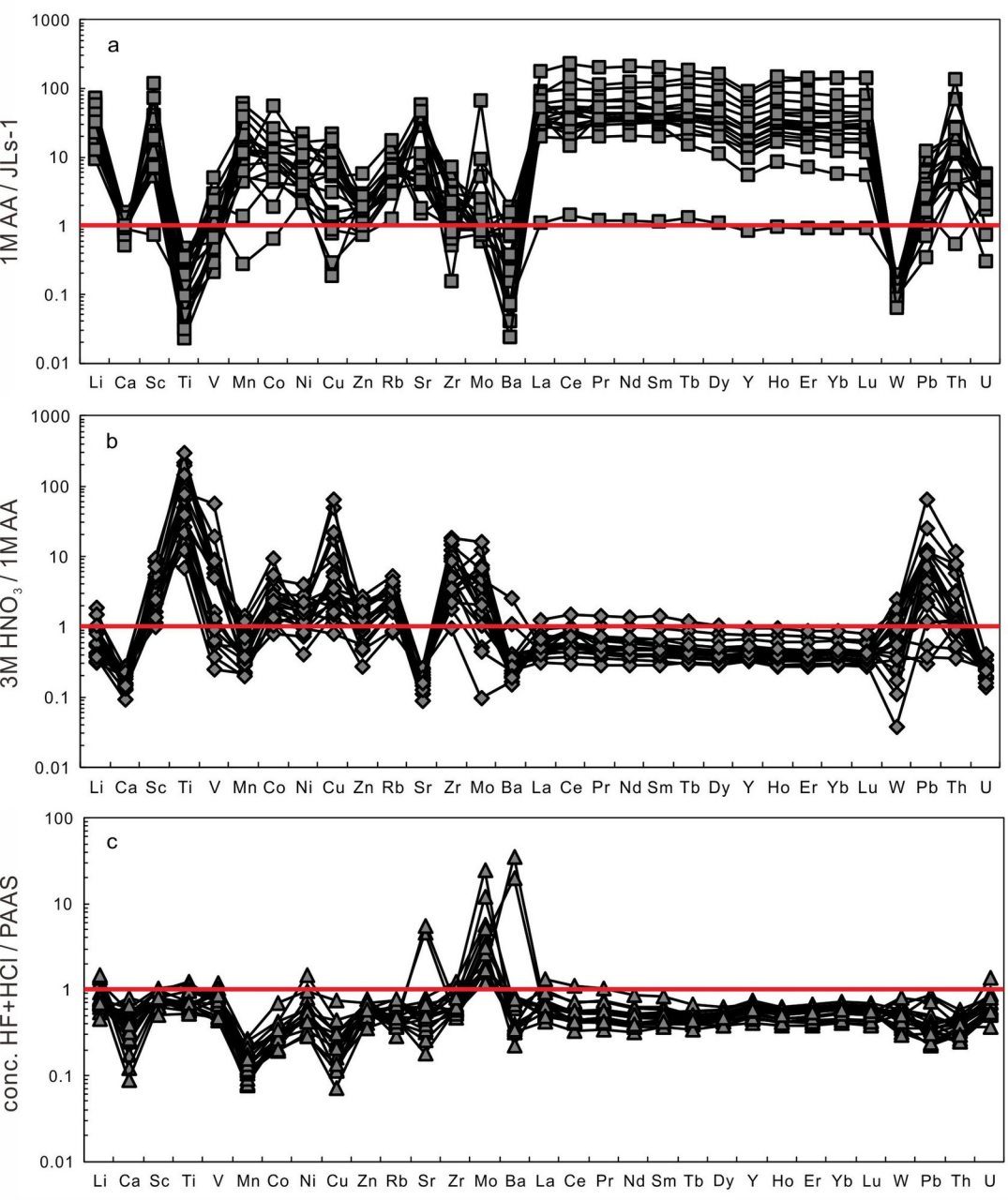
a
1M AA / JLs-1
1000
100
10
1
0.1
0.01
Li Ca Sc Ti V Mn Co Ni Cu Zn Rb Sr Zr Mo Ba La Ce Pr Nd Sm Tb Dy Y Ho Er Yb Lu W Pb Th U
b
3M HNO3 / 1M AA
1000
100
10
1
0.1
0.01
Li Ca Sc Ti V Mn Co Ni Cu Zn Rb Sr Zr Mo Ba La Ce Pr Nd Sm Tb Dy Y Ho Er Yb Lu W Pb Th U
c
conc. HF+HCl / PAAS
100
10
1
0.1
0.01
Li Ca Sc Ti V Mn Co Ni Cu Zn Rb Sr Zr Mo Ba La Ce Pr Nd Sm Tb Dy Y Ho Er Yb Lu W Pb Th U

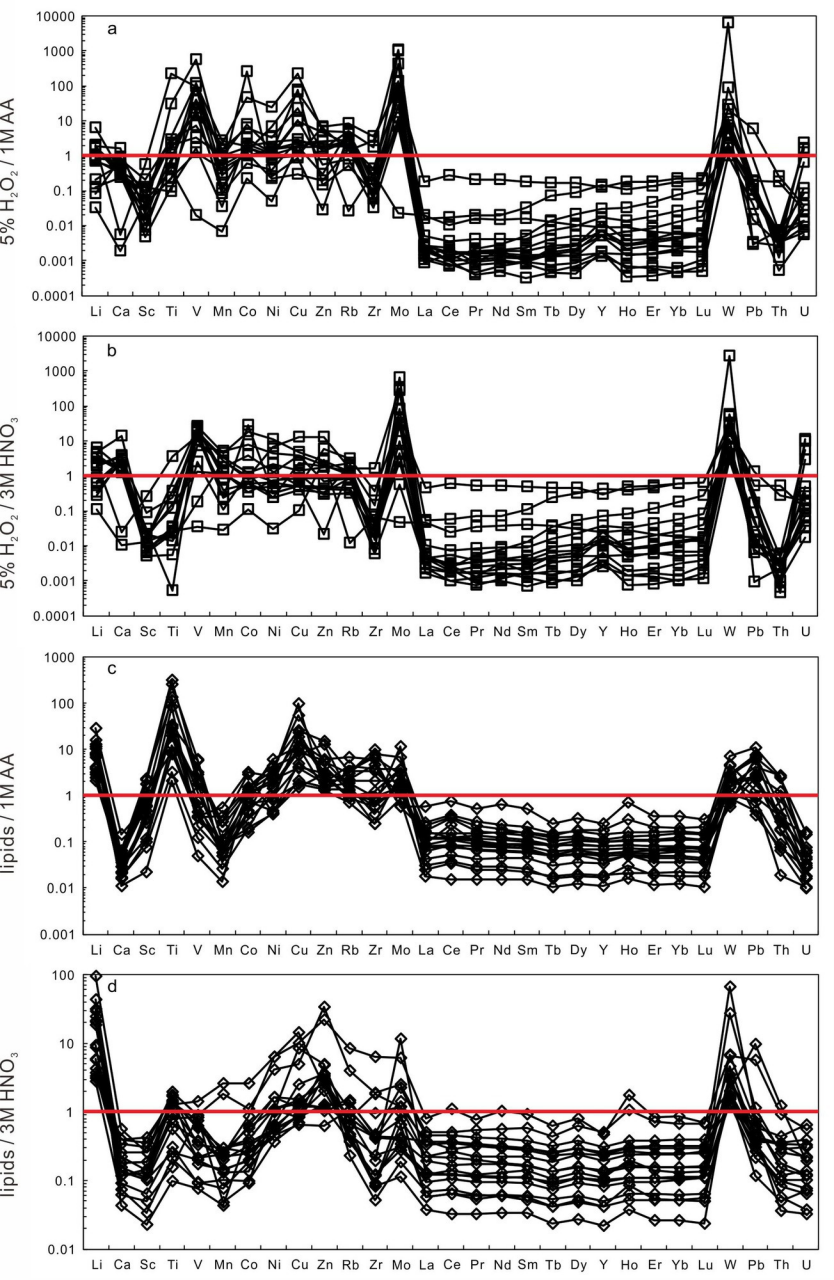
a
5% H2O2 / 1M AA
b
5% H2O2 / 3M HNO3
c
lipids / 1M AA
d
lipids / 3M HNO3
Li Ca Sc Ti V Mn Co Ni Cu Zn Rb Zr Mo La Ce Pr Nd Sm Tb Dy Y Ho Er Yb Lu W Pb Th U

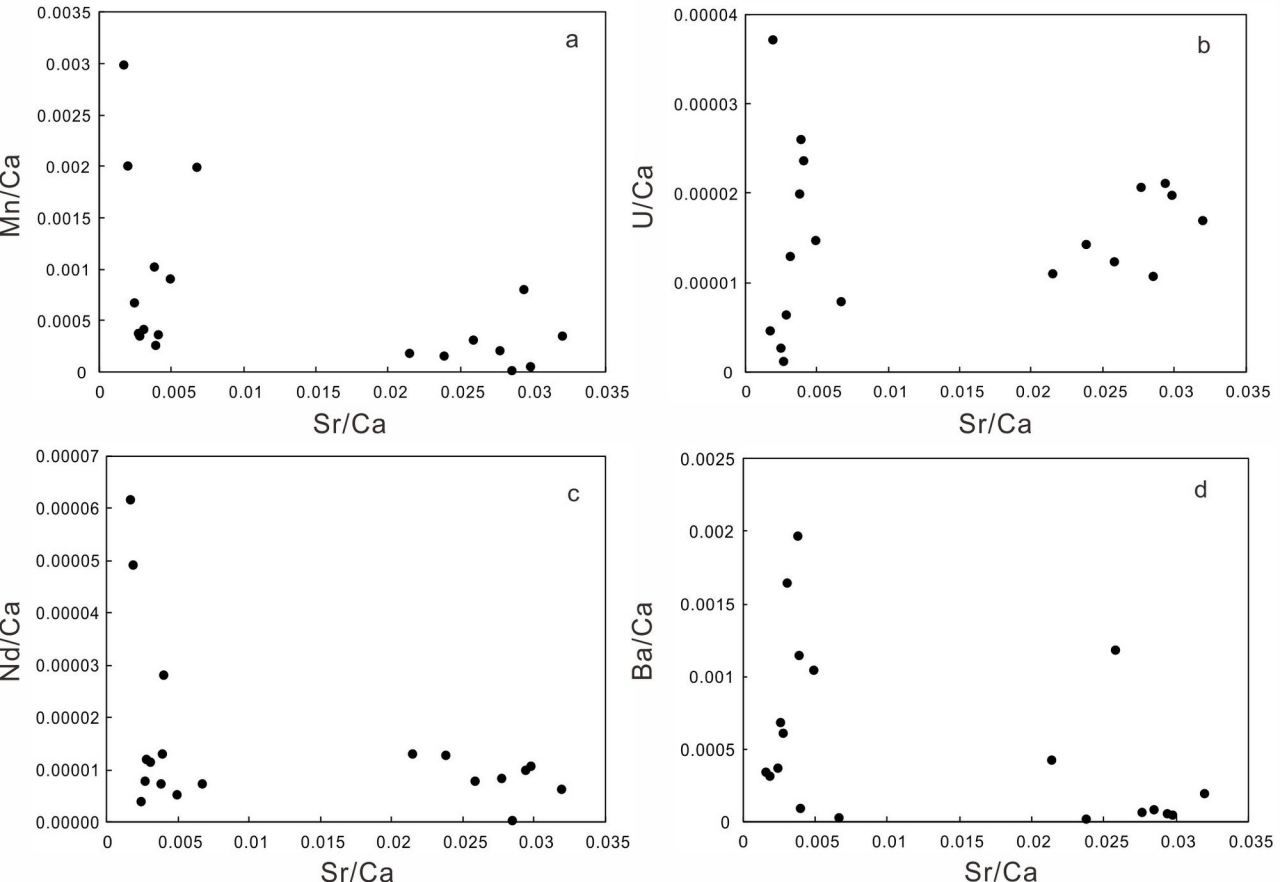
a
Mn/Ca
Sr/Ca
0.0035
0.003
0.0025
0.002
0.0015
0.001
0.0005
0
0.005
0.01
0.015
0.02
0.025
0.03
0.035
b
U/Ca
0.00004
0.00003
0.00002
0.00001
c
Nd/Ca
0.00007
0.00006
0.00005
0.00004
0.00003
0.00002
0.00001
0.00000
d
Ba/Ca
0.0025
0.002
0.0015
0.001
0.0005

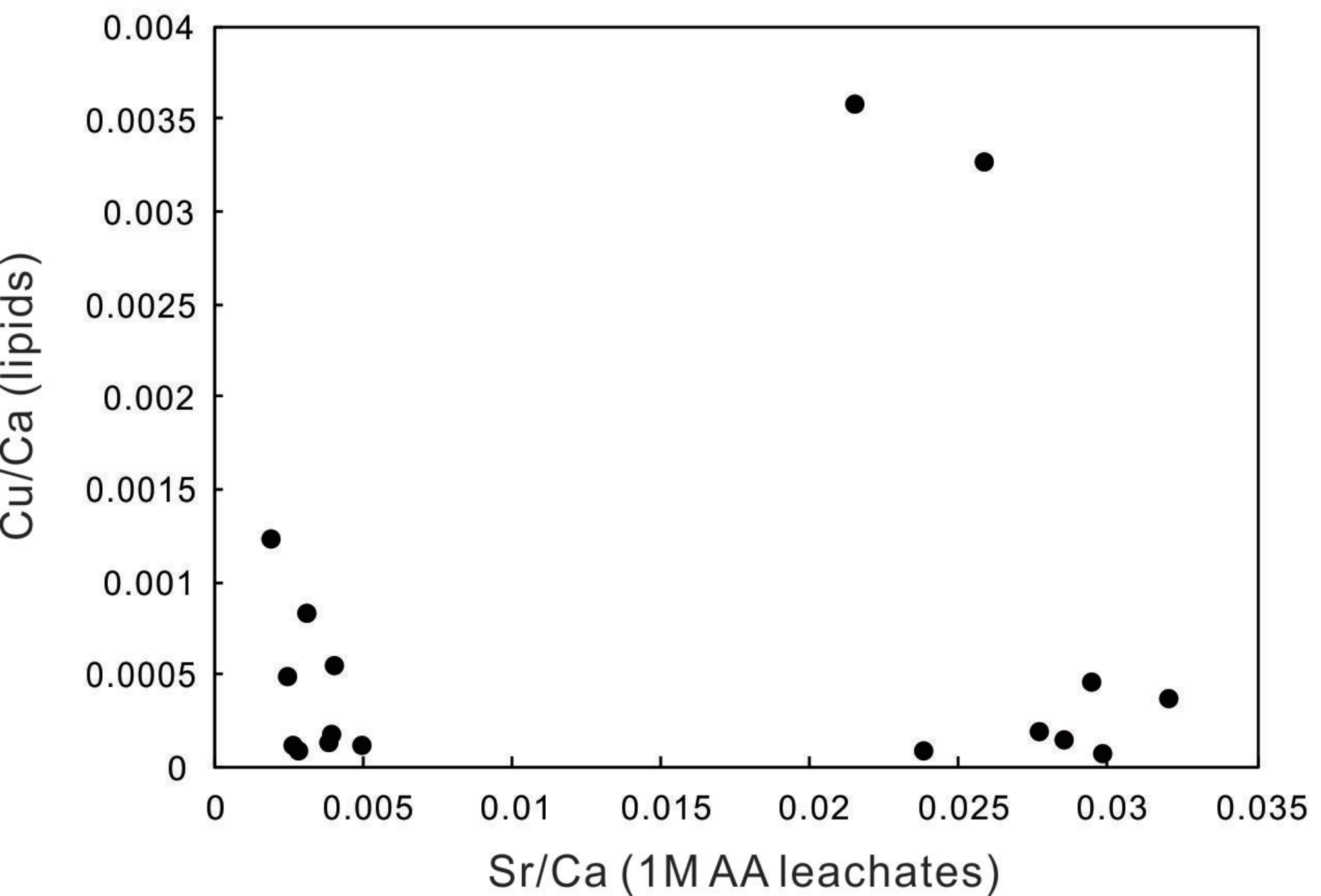
0.004
0.0035
0.003
0.0025
0.002
0.0015
0.001
0.0005
0
Cu/Ca (lipids)
0
0.005
0.01
0.015
0.02
0.025
0.03
0.035
Sr/Ca (1M AA leachates)

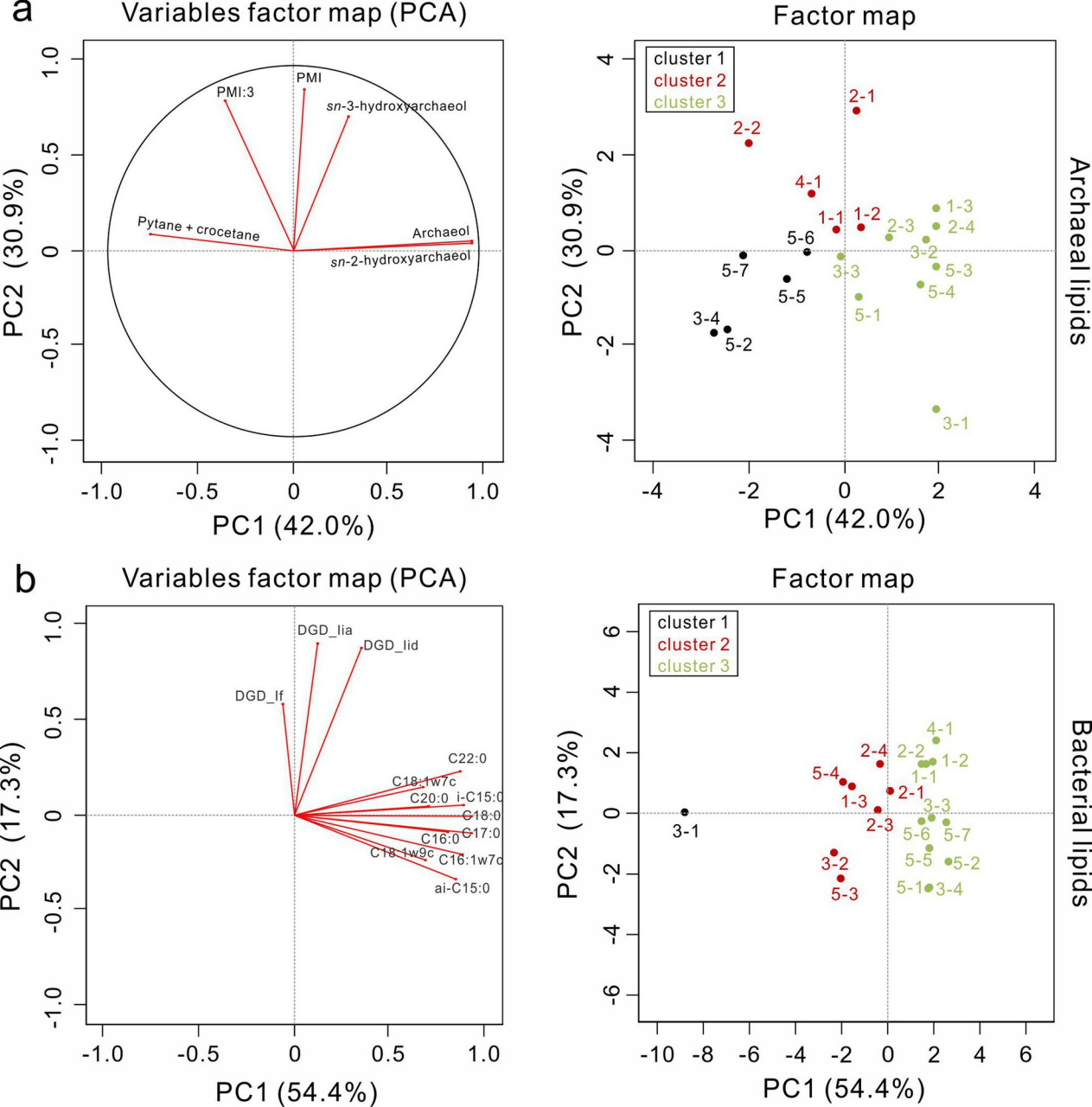
a
Variables factor map (PCA)
PMI:3
PMI
sn-3-hydroxyarchaeol
Pytane + crocetane
Archaeol
sn-2-hydroxyarchaeol
PC2 (30.9%)
PC1 (42.0%)
Factor map
cluster 1
cluster 2
cluster 3
Archaeal lipids
b
Variables factor map (PCA)
DGD_lia
DGD_lid
DGD_lf
C22:0
C18:1w7c
C20:0
i-C15:0
C18:0
C16:0
C17:0
C18:1w9c
C16:1w7c
ai-C15:0
PC2 (17.3%)
PC1 (54.4%)
Factor map
cluster 1
cluster 2
cluster 3
Bacterial lipids

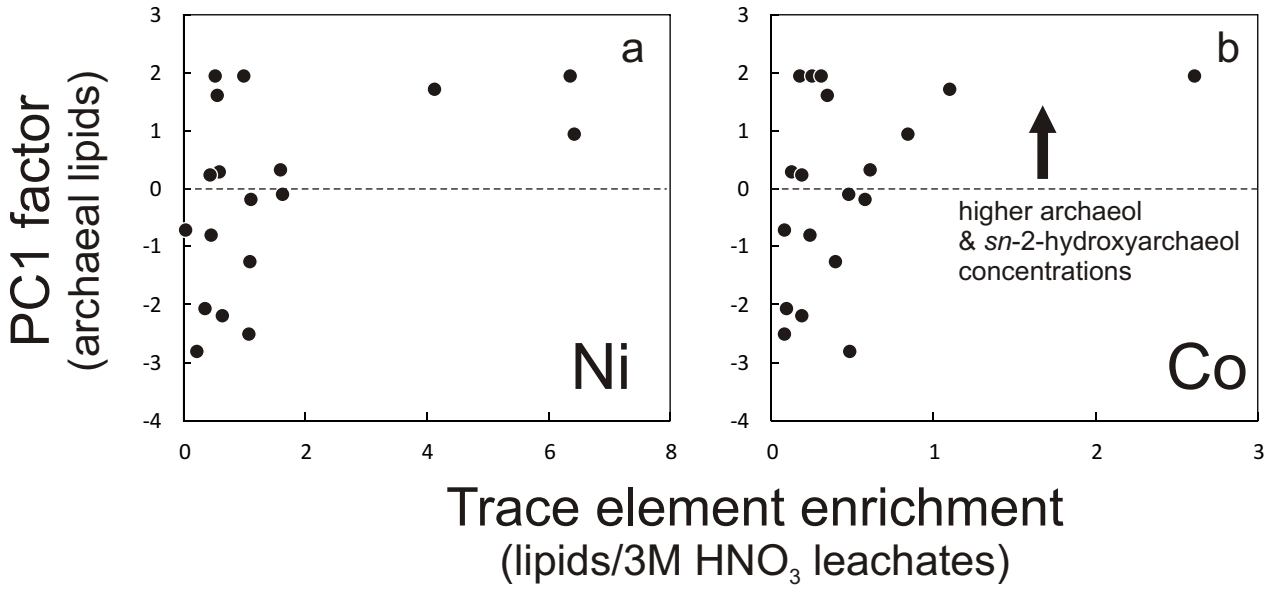
PC1 factor
(archaeal lipids)
a
Ni
b
Co
higher archaeol
& *sn*-2-hydroxyarchaeol
concentrations
Trace element enrichment
(lipids/3M HNO_3 leachates)

Table 1 Site information, water depth, mineral compositions, and carbon and oxygen stable isotopic compassions of the seep carbonate analyzed in this study

					C and O isotopes		Mineral composition			
Sites	Area	Old ID	New ID	water depth (m)	$\delta^{13}C$ (‰)	$\delta^{18}O$ (‰)	Arag. (wt %)	Cal. (wt %)	Dolo. (wt %)	cited from
1	Congo Fan	ZR2-PL13-P04	1-1	2830	-58.5	5.3		>50%		Pierre and Fouquet, 2007
		ZR2-PL14-P05	1-2	3150	-53.6	5.6		>50%		
		BZ1-GBT3-PL7-83	1-3	3150	-49.5	2.9		>50%		
2	Nile Deep-Sea Fan	NL4-CC1	2-1	2875-3032	-38.9	2.8	72.0	4.0	1.0	Gontharet et al., 2007
		NL7-CC1	2-2	1683-2132	-41.8	4.2	0.0	51.0	27.0	
		NL14-CC5	2-3	1683-2132	-29.2	3.2	70.0	20.0		
		NL20-CC1	2-4	2875-3032	-38.4	3.1	82.0	5.0		
3	Niger Fan	N1-KS-07	3-1	1633	-45.9	4.0	87.4	11.5		Rongemaille et al., 2011
		N1-KS-22	3-2	1150	-27.8	4.9	90.4	9.8		
		N1-KSF-45	3-3	1546	-47.1	6.1		5.7	87.3	
		N1-KI-47	3-4	1540	-48.0	5.7		7.7	86.3	
4	eastern Mediterranean Sea	MN13BT6-1	4-1	~2000	-31.0	3.9	86.8	4.1		Aloisi et al., 2000
5	Gulf of Mexico	#2 4173-2 (AT340)	5-1	2216	-54.2	4.0	62.5			Feng et al., 2010
		#7 4174-2 (GC600)	5-2	1250	-21.4	4.8		52.3		Roberts et al., 2010
		#65 271-1 (MC462)	5-3	973	-40.5	4.6	79.8			Feng et al., unpublised data
		#67 272-1 (GC415)	5-4	1110	-38.2	3.4		68.4	1.1	Feng and Roberts, 2011
		#68 273-1 (GC852)	5-5		-40.2	3.7		69.8	1.2	
		#69 273-2 (GC852)	5-6	1633	-40.1	3.7		62.0	1.5	Roberts et al., 2010
		#70 273-3 (GC852)	5-7		-48.1	4.5		54.3	1.7	

Table 2 element concentrations (mg/kg) for BHVO-2 and JLs-1

element	BHVO-2	JLs-1	
	Reference values[a]	This study	RSD (%)
Li	4.7	0.07	11.8
Ca	81429[b]	403500[c]	—
Sc	32.3	0.019	7.8
Ti	16364	2.75	61.0
V	317	3.00	2.4
Mn	1290	14.68	2.4
Co	45	0.045	4.9
Ni	121	0.30	4.6
Cu	123	0.15	7.3
Zn	101	2.09	2.6
Rb	9.08	0.10	5.5
Sr	396	274	2.3
Y	27.6	0.24	0.4
Zr	164.9	0.14	17.0
Mo	4.07[b]	0.079	3.3
Ba	131	432	2.6
La	15.2	0.094	2.6
Ce	37.5	0.171	3.1
Pr	5.31	0.021	1.8
Nd	24.5	0.084	0.7
Sm	6.07	0.019	1.5
Tb	0.94	0.003	1.8
Dy	5.31	0.019	1.6
Ho	1.00	0.005	3.4
Er	2.54	0.014	4.4
Tm	0.34	—	—
Yb	2.00	0.012	3.2
Lu	0.27	0.002	2.2
W	0.22	0.10	3.5
Pb	1.51	0.08	9.1
Th	1.21	0.017	2.6
U	0.41	1.68	1.1

a: from Barrat et al. (2012)
b: from Jochum et al. (2016)
c: from Straaten et al. (2008)

Table 3 Element concentrations for inorganic and organic fractions of cold seep carbonates (mg/kg)

1M AA leachates

New ID	Li	Ca	Sc	Ti	V	Mn	Co	Ni	Cu	Zn	Rb	Sr	Zr	Mo	Ba
1-1	4.16	405,389	0.12	0.64	3.16	412.6	0.19	1.14	0.12	4.42	0.64	1,535	0.10	0.71	798
1-2	2.86	289,087	0.18	0.60	7.48	76.4	0.19	0.75	0.04	1.83	0.34	1,121	0.11	0.41	330
1-3	3.22	437,326	0.26	0.56	1.63	70.1	0.75	3.00	0.19	2.86	0.32	10,409	0.13	0.07	10
2-1	1.29	332,078	0.38	0.31	8.79	265.5	0.54	1.90	0.24	3.87	0.76	9,753	0.77	0.18	18
2-2	3.31	318,397	0.72	1.27	1.77	117.4	2.42	3.82	1.92	3.94	0.57	1,281	0.41	0.06	30
2-3	2.10	355,634	0.64	0.97	3.68	63.5	0.29	1.59	3.34	5.07	0.50	7,619	0.41	0.05	152
2-4	1.39	374,142	0.27	0.92	3.30	114.9	0.38	0.93	1.96	2.84	0.37	9,657	0.58	0.06	444
3-1	0.62	370,540	0.01	0.30	4.67	3.9	0.03	0.72	0.21	1.53	0.12	10,563	0.02	5.13	32
3-2	1.12	346,842	0.11	0.36	6.25	19.8	0.22	0.63	0.13	1.50	0.30	10,327	0.08	0.71	17
3-3	3.01	209,436	2.18	0.53	14.46	419.4	0.33	1.05	0.03	6.12	1.11	395	0.47	0.19	65
3-4	4.90	294,943	1.32	0.13	0.69	880.2	1.14	6.28	0.80	11.76	1.71	485	0.14	0.07	100
4-1	1.50	364,923	0.30	0.18	0.63	727.6	0.81	4.98	2.71	3.07	0.28	2,442	0.10	0.06	10
5-1	0.84	483,551	0.21	0.21	1.20	167.4	0.54	1.60	0.90	2.07	0.92	15,455	0.45	0.07	92
5-2	2.12	440,932	0.13	0.14	1.64	294.9	0.52	1.25	0.46	3.68	0.71	1,074	0.44	0.12	162
5-3	0.83	449,033	0.10	0.06	0.83	91.0	0.08	4.32	1.68	2.64	0.47	12,430	0.34	0.13	31
5-4	3.88	623,116	0.13	0.09	1.39	564.1	0.60	4.73	1.23	5.44	0.74	3,051	0.12	0.09	652
5-5	2.27	429,953	0.13	0.26	2.21	160.1	0.51	1.67	0.85	3.35	0.59	1,141	0.34	0.06	295
5-6	2.77	521,271	0.13	0.09	1.95	181.9	0.53	3.19	1.19	3.52	0.71	1,445	0.20	0.06	318
5-7	2.14	398,997	0.35	0.94	6.90	166.7	0.42	1.18	0.85	3.86	0.64	1,228	1.08	0.07	657

New ID	La	Ce	Pr	Nd	Sm	Tb	Dy	Y	Ho	Er	Yb	Lu	W	Pb	Th	U
1-1	2.23	8.21	0.70	2.92	0.64	0.10	0.59	4.28	0.13	0.40	0.38	0.06	0.02	0.50	0.37	8.07
1-2	3.24	8.50	0.89	3.80	0.82	0.14	0.87	6.43	0.20	0.59	0.52	0.08	0.01	0.11	0.42	7.50
1-3	5.65	11.69	1.37	5.53	0.93	0.10	0.53	3.51	0.11	0.28	0.22	0.03	0.02	0.08	0.47	6.23
2-1	3.10	6.80	0.77	3.29	0.69	0.11	0.64	4.06	0.13	0.36	0.31	0.05	0.01	0.11	0.31	7.02
2-2	8.41	16.56	2.06	8.91	2.00	0.33	1.98	13.18	0.41	1.12	0.92	0.14	0.01	0.81	0.40	7.50
2-3	4.44	6.85	1.07	4.59	0.99	0.17	1.06	9.06	0.23	0.65	0.53	0.08	0.01	1.01	0.36	3.93
2-4	2.63	4.38	0.66	2.94	0.65	0.11	0.67	5.58	0.15	0.41	0.33	0.05	0.01	0.49	0.20	4.58
3-1	0.10	0.24	0.02	0.10	0.02	0.00	0.02	0.20	0.00	0.01	0.01	0.00	0.02	0.13	0.01	3.95
3-2	4.36	9.48	0.91	3.73	0.55	0.04	0.21	1.25	0.04	0.09	0.07	0.01	0.01	0.40	0.19	6.88
3-3	7.70	24.62	2.33	10.30	2.32	0.41	2.61	18.20	0.59	1.78	1.67	0.25	0.01	0.32	1.20	7.77

3-4	15.97	39.61	4.25	18.13	3.73	0.53	3.07	21.00	0.65	1.86	1.64	0.25	0.01	0.18	2.31	1.36
4-1	2.52	4.55	0.62	2.67	0.61	0.10	0.59	4.17	0.12	0.33	0.26	0.04	0.01	0.14	0.19	2.89
5-1	3.31	4.88	0.73	3.06	0.62	0.08	0.47	3.12	0.10	0.25	0.20	0.03	0.01	0.11	0.21	8.21

Table 3 (*continued*)

New ID	La	Ce	Pr	Nd	Sm	Tb	Dy	Y	Ho	Er	Yb	Lu	W	Pb	Th	U
5-2	1.84	3.17	0.41	1.74	0.38	0.06	0.37	3.00	0.08	0.23	0.21	0.03	0.01	0.03	0.07	1.19
5-3	3.83	2.43	0.85	3.73	0.66	0.07	0.38	2.32	0.07	0.19	0.14	0.02	0.01	0.29	0.08	9.30
5-4	2.90	3.60	0.70	3.20	0.75	0.12	0.69	5.49	0.15	0.39	0.31	0.05	0.01	0.06	0.07	9.13
5-5	3.33	4.54	0.77	3.39	0.75	0.12	0.73	5.62	0.16	0.43	0.35	0.05	0.01	0.13	0.09	0.50
5-6	5.99	5.92	1.39	6.26	1.42	0.24	1.42	11.07	0.31	0.83	0.64	0.10	0.01	0.22	0.09	3.35
5-7	4.94	9.38	1.11	4.53	0.95	0.15	0.88	6.20	0.19	0.52	0.46	0.07	0.01	0.14	0.44	5.17

3M HNO_3 leachates

New ID	Li	Ca	Sc	Ti	V	Mn	Co	Ni	Cu	Zn	Rb	Sr	Zr	Mo	Ba
1-1	1.28	78,284	0.49	9.51	1.85	94.8	0.37	1.94	2.05	3.81	1.32	276	0.48	0.36	862
1-2	1.18	76,201	0.54	11.78	4.18	37.9	0.47	1.61	2.06	3.51	1.27	276	0.56	0.44	110
1-3	1.72	84,464	0.76	19.23	9.27	19.9	0.58	2.16	1.13	5.13	1.01	1,757	0.66	0.36	4
2-1	0.70	82,870	0.80	15.11	10.92	107.5	1.87	3.38	5.07	4.98	1.53	1,967	4.01	2.16	5
2-2	1.39	57,396	1.15	33.08	11.93	99.9	3.84	4.44	4.11	3.34	1.21	229	3.72	0.21	10
2-3	0.82	77,181	0.72	20.93	5.83	19.9	0.32	1.53	2.59	2.85	0.85	1,534	1.23	0.05	42
2-4	0.79	86,172	0.60	14.75	4.31	38.6	0.39	1.54	2.40	2.57	0.78	1,958	1.63	0.27	1110
3-1	0.23	100,187	0.12	2.01	1.15	0.8	0.03	0.29	0.32	0.41	0.10	2,660	0.02	0.49	5
3-2	0.34	91,331	0.26	4.27	2.31	3.8	0.30	0.66	0.68	0.69	0.25	2,302	0.13	0.31	4
3-3	0.98	51,783	2.10	11.50	9.29	138.1	0.83	1.89	1.81	2.93	1.83	74	1.43	1.41	19
3-4	1.96	37,088	1.80	10.86	37.56	445.3	2.30	7.34	2.91	12.32	4.34	54	1.73	0.12	40
4-1	1.34	77,301	0.64	11.59	4.41	211.3	2.34	13.65	5.09	3.52	0.76	436	0.97	0.14	3
5-1	1.58	73,994	0.64	18.57	10.78	91.5	1.26	2.44	3.13	5.24	2.14	2,193	2.23	0.34	20
5-2	3.18	115,006	1.17	29.58	11.11	221.3	2.47	4.98	4.13	9.57	3.58	280	6.51	0.78	57
5-3	0.80	101,206	0.41	11.98	4.68	127.8	0.76	3.39	2.67	3.45	1.08	2,325	0.76	0.26	8
5-4	1.43	56,505	0.63	13.71	26.48	199.3	1.30	3.89	2.97	6.77	1.51	270	2.22	1.48	100
5-5	1.95	68,590	0.69	19.85	10.82	111.8	1.43	3.38	2.26	6.11	1.94	179	2.87	0.09	57
5-6	2.20	68,360	0.92	24.58	16.41	218.7	2.91	5.73	3.26	7.76	2.30	184	3.41	0.13	60
5-7	2.21	57,763	0.85	36.44	6.36	60.0	0.98	2.63	2.96	6.17	2.72	191	3.67	0.46	126

New ID	La	Ce	Pr	Nd	Sm	Tb	Dy	Y	Ho	Er	Yb	Lu	W	Pb	Th	U
1-1	1.00	3.46	0.30	1.20	0.25	0.03	0.20	1.52	0.04	0.13	0.13	0.02	0.0006	0.56	0.47	1.52
1-2	1.70	4.54	0.46	1.88	0.39	0.06	0.39	3.09	0.09	0.25	0.24	0.03	0.0014	0.58	0.54	1.99
1-3	2.25	5.21	0.54	2.06	0.35	0.04	0.21	1.48	0.04	0.11	0.09	0.01	0.0046	0.80	0.71	1.55
2-1	2.83	6.67	0.79	3.21	0.65	0.09	0.51	3.13	0.10	0.26	0.21	0.03	0.0021	0.81	0.51	1.73

Table 3 (*continued*)

New ID	La	Ce	Pr	Nd	Sm	Tb	Dy	Y	Ho	Er	Yb	Lu	W	Pb	Th	U
2-2	3.60	8.80	0.87	3.58	0.75	0.12	0.67	5.09	0.14	0.38	0.32	0.05	0.0098	1.91	0.44	1.90
2-3	1.57	2.55	0.38	1.56	0.32	0.05	0.30	2.90	0.06	0.17	0.15	0.02	0.0079	0.54	0.18	0.93
2-4	1.43	2.51	0.35	1.45	0.30	0.04	0.26	2.30	0.05	0.14	0.12	0.02	0.0079	0.57	0.23	1.21
3-1	0.08	0.16	0.02	0.06	0.01	0.00	0.01	0.10	0.00	0.01	0.00	0.00	0.0078	0.04	0.01	1.54
3-2	1.31	2.75	0.26	1.04	0.16	0.01	0.06	0.45	0.01	0.03	0.02	0.00	0.0039	0.15	0.07	1.74
3-3	3.65	11.76	1.10	4.73	1.04	0.18	1.17	9.18	0.26	0.79	0.76	0.11	0.0050	0.64	0.63	2.58
3-4	7.73	20.59	2.06	8.37	1.69	0.23	1.34	9.51	0.28	0.79	0.74	0.11	0.0075	1.96	1.90	0.39
4-1	1.03	2.04	0.25	1.05	0.23	0.04	0.21	1.79	0.04	0.11	0.10	0.01	0.0118	0.60	0.17	0.56
5-1	2.14	3.96	0.51	2.02	0.41	0.06	0.29	2.03	0.06	0.15	0.12	0.02	0.0150	1.39	0.65	1.48
5-2	2.27	4.69	0.59	2.39	0.52	0.07	0.38	2.89	0.08	0.20	0.18	0.03	0.0147	1.79	0.82	0.48
5-3	1.57	2.17	0.36	1.45	0.26	0.03	0.16	1.20	0.03	0.08	0.07	0.01	0.0225	0.93	0.23	1.80
5-4	1.79	3.32	0.46	1.87	0.39	0.06	0.31	2.40	0.06	0.17	0.15	0.02	0.0164	1.43	0.52	1.28
5-5	1.96	3.70	0.49	1.98	0.42	0.06	0.33	2.65	0.07	0.18	0.15	0.02	0.0122	1.47	0.51	0.12
5-6	3.06	5.35	0.74	3.06	0.66	0.10	0.56	4.61	0.12	0.31	0.26	0.04	0.0104	2.53	0.67	0.54
5-7	3.30	6.68	0.79	3.10	0.62	0.08	0.45	3.23	0.09	0.24	0.21	0.03	0.0056	1.42	0.83	1.22

Detrital fractions

New ID	Li	Ca	Sc	Ti	V	Mn	Co	Ni	Cu	Zn	Rb	Sr	Zr	Mo	Ba
1-1	93.6	4,371	11.5	3,453	65.0	70.1	6.08	24.0	12.6	45.4	70	931	98	1.67	22,659
1-2	101.3	1,335	12.0	4,052	74.4	64.2	6.50	25.8	11.5	43.8	72	35	125	1.56	257
1-3	107.5	947	11.5	4,421	80.5	68.2	5.83	44.4	15.3	59.0	64	63	135	4.31	396
2-1	52.0	4,073	15.5	7,421	109.0	103.4	7.75	33.9	8.1	52.7	46	163	261	5.69	204
2-2	57.7	4,699	16.5	6,905	123.6	227.9	15.93	52.2	37.2	59.2	61	91	213	24.75	209
2-3	57.6	3,466	16.0	5,832	119.9	129.2	7.82	34.7	15.7	47.7	62	113	217	1.86	231
2-4	41.2	6,165	10.5	4,062	65.0	106.2	6.13	27.2	11.4	44.0	59	1,091	144	3.96	13,128

3-3	109.4	1,890	12.8	5,623	109.0	77.4	6.73	30.3	5.9	45.7	78	92	183	5.19	239
3-4	68.4	679	10.0	3,291	176.8	210.7	9.58	31.9	5.6	66.7	68	52	118	3.31	144
4-1	55.2	3,123	16.0	4,227	99.4	162.1	9.25	80.2	22.3	47.6	80	69	128	2.59	218
5-1	46.5	3,722	11.9	3,588	154.7	90.8	4.45	16.0	5.7	42.0	102	143	116	1.22	511
5-2	54.9	2,074	12.9	3,065	120.7	97.9	4.37	16.8	3.5	34.7	111	80	109	1.69	497
5-3	49.9	3,256	12.5	3,711	132.9	100.1	4.80	28.6	21.7	47.6	102	125	123	3.12	478
5-4	59.5	2,648	12.5	3,911	133.8	177.6	6.83	29.8	12.1	58.2	120	93	125	12.18	441
5-5	51.4	2,503	12.4	3,360	110.5	117.2	6.03	18.5	10.3	41.3	107	90	129	1.21	547
5-6	53.2	3,065	12.6	4,096	130.6	145.2	7.87	23.2	15.3	49.1	123	97	131	1.81	500

Table 3 (*continued*)

New ID	Li	Ca	Sc	Ti	V	Mn	Co	Ni	Cu	Zn	Rb	Sr	Zr	Mo	Ba
5-7	34.0	5,087	8.1	3,164	71.5	132.8	4.63	15.7	6.8	30.3	76	134	168	1.68	510

New ID	La	Ce	Pr	Nd	Sm	Tb	Dy	Y	Ho	Er	Yb	Lu	W	Pb	Th	U
1-1	24.40	35.50	4.20	13.89	2.41	0.30	1.81	10.94	0.37	1.09	1.14	0.17	1.44	9.80	5.41	4.23
1-2	24.10	34.92	4.16	13.72	2.34	0.33	1.98	12.89	0.41	1.23	1.30	0.19	1.59	10.18	5.59	1.95
1-3	38.62	55.56	6.56	21.53	3.47	0.39	2.16	12.10	0.41	1.16	1.13	0.16	1.79	17.14	8.52	2.53
2-1	28.31	43.31	4.96	16.96	2.91	0.42	2.76	20.34	0.61	1.89	2.05	0.30	1.58	5.86	3.60	1.60
2-2	16.20	25.97	3.05	10.83	2.02	0.35	2.29	15.97	0.50	1.54	1.65	0.24	1.56	8.44	3.94	1.71
2-3	26.90	45.32	5.10	17.82	3.07	0.43	2.73	18.90	0.59	1.77	1.91	0.28	1.21	7.60	6.77	2.14
2-4	19.67	32.94	3.73	13.11	2.31	0.33	2.11	14.54	0.46	1.39	1.50	0.22	0.97	7.12	3.61	1.57
3-3	51.02	89.50	8.98	29.57	4.63	0.52	2.98	18.01	0.61	1.77	1.82	0.27	1.33	16.61	7.38	1.89
3-4	35.20	57.90	6.27	20.56	3.26	0.37	2.09	12.20	0.42	1.21	1.25	0.19	2.16	14.64	5.45	1.14
4-1	20.48	35.68	3.90	13.39	2.15	0.30	1.96	13.86	0.44	1.38	1.51	0.22	2.20	4.58	4.73	1.83
5-1	19.11	33.25	3.66	12.65	2.02	0.27	1.78	12.93	0.41	1.32	1.48	0.22	1.01	4.42	4.28	1.95
5-2	24.67	45.29	4.92	16.95	2.64	0.34	2.24	15.39	0.51	1.59	1.74	0.26	0.87	4.77	5.37	2.74
5-3	24.25	41.85	4.65	16.02	2.56	0.34	2.23	15.63	0.50	1.56	1.72	0.25	1.36	7.65	7.34	2.65
5-4	25.05	44.53	4.82	16.55	2.64	0.36	2.36	16.39	0.53	1.65	1.79	0.26	1.39	6.16	5.57	2.24
5-5	24.19	45.22	4.87	16.96	2.74	0.38	2.53	17.14	0.56	1.73	1.84	0.27	1.16	6.87	6.35	2.48
5-6	24.85	45.51	4.95	17.25	2.80	0.39	2.57	17.79	0.57	1.77	1.88	0.28	1.39	7.03	5.75	2.53
5-7	18.61	34.02	3.78	13.44	2.34	0.34	2.23	15.51	0.50	1.54	1.65	0.24	0.80	6.16	4.25	1.67

5% H_2O_2 leachates

New ID	Li	Ca	Sc	Ti	V	Mn	Co	Ni	Cu	Zn	Rb	Sr	Zr	Mo	Ba
1-1	0.14	784	0.01	0.25	0.06	2.75	0.04	0.06	0.21	10.8	0.02	4.9	0.03	0.02	2.32
1-2	2.28	267,484	0.01	1.38	107	171	8.89	18.3	9.48	9.67	1.62	525	0.02	19.7	52.4
1-3	5.19	148,388	0.01	0.46	68.0	103	4.67	9.64	4.46	3.65	0.86	442	0.03	28.2	72.6
2-1	2.36	108,335	0.01	0.51	156	26.2	1.13	2.23	2.39	2.11	0.61	1,935	0.02	1.19	2.59
2-2	2.86	226,833	0.01	0.74	214	323	4.65	9.37	5.69	5.99	2.85	4,980	0.06	57.1	8.20
2-3	3.43	97,444	0.00	0.69	136	17.0	0.36	0.36	1.00	0.96	0.74	359	0.03	1.33	4.98
2-4	2.45	158,338	0.01	0.21	75.5	9.33	0.23	0.37	5.73	4.90	0.99	2,612	0.04	0.68	37.2
3-2	0.09	275,657	0.02	1.02	45.3	10.4	0.28	4.40	8.77	9.13	0.42	6,319	0.21	96.9	36.1
3-3	0.61	119,234	0.01	0.06	22.8	15.1	1.03	1.31	2.08	0.87	0.57	3,240	0.04	13.6	6.02
3-4	9.13	497,185	0.03	4.00	387	793	8.97	9.66	1.47	3.56	8.87	780	0.25	79.1	66.2
4-1	3.04	1,924	0.17	41.3	62.3	83.0	1.45	4.42	2.68	20.7	2.41	13.6	0.35	4.78	8.63

Table 3 (*continued*)

New ID	Li	Ca	Sc	Ti	V	Mn	Co	Ni	Cu	Zn	Rb	Sr	Zr	Mo	Ba
5-3	5.12	159,575	0.01	0.01	99.6	29.3	21.65	1.08	1.39	0.07	1.93	2,148	0.03	1.16	6.5
5-4	0.49	147,453	0.01	0.19	4.8	549.9	1.03	4.63	11.71		1.61	3,179	0.05	6.10	21.9
5-5	1.66	132,791	0.01		265.1	135.4	0.49	2.51	1.94		1.63	500	0.02	7.54	69.4
5-7	1.50	161,386	0.01		8.7	69.9	0.45	1.29	1.52		1.22	315	0.06	1.83	40.1

New ID	La	Ce	Pr	Nd	Sm	Tb	Dy	Y	Ho	Er	Yb	Lu	W	Pb	Th	U
1-1	0.0449	0.0820	0.0107	0.0442	0.0099	0.0012	0.0063	0.0374	0.0012	0.0028	0.0023	0.0003	0.03	0.09	0.00	0.05
1-2	0.0091	0.0120	0.0016	0.0077	0.0019	0.0006	0.0043	0.0318	0.0013	0.0048	0.0064	0.0014	0.03	0.00	0.00	0.61
1-3	0.0131	0.0118	0.0029	0.0163	0.0046	0.0013	0.0111	0.1029	0.0034	0.0128	0.0168	0.0035	0.03	0.01	0.00	0.75
2-1	0.0083	0.0119	0.0013	0.0052	0.0010	0.0002	0.0009	0.0202	0.0002	0.0006	0.0007	0.0001	0.11	0.01	0.00	0.09
2-2	0.0154	0.0160	0.0022	0.0105	0.0023	0.0006	0.0043	0.0674	0.0011	0.0037	0.0039	0.0007	0.03	0.09	0.00	0.20
2-3	0.0068	0.0136	0.0014	0.0066	0.0012	0.0002	0.0015	0.0143	0.0003	0.0010	0.0010	0.0001	0.09	0.00	0.00	0.15
2-4	0.0066	0.0077	0.0011	0.0054	0.0012	0.0003	0.0019	0.0391	0.0004	0.0015	0.0016	0.0003	0.03	0.01	0.00	0.04
3-2	0.0683	0.1597	0.0179	0.0735	0.0176	0.0031	0.0185	0.1831	0.0042	0.0126	0.0118	0.0019	0.13	0.08	0.03	0.20
3-3	0.0209	0.0249	0.0009	0.0048	0.0007	0.0002	0.0011	0.0318	0.0002	0.0006	0.0008	0.0001	0.01	0.01	0.00	0.04
3-4	0.0809	0.1438	0.0176	0.0748	0.0152	0.0037	0.0304	0.3506	0.0092	0.0343	0.0438	0.0088	0.08	0.03	0.01	2.16
4-1	0.4650	1.2438	0.1292	0.5348	0.1106	0.0164	0.0979	0.5309	0.0211	0.0595	0.0590	0.0087	0.23	0.80	0.05	0.11
5-3	0.0033	0.0037	0.0006	0.0031	0.0006	0.0002	0.0010	0.0296	0.0003	0.0008	0.0009	0.0001	61.96	0.00	0.00	0.13
5-4	0.0076	0.0086	0.0006	0.0063	0.0007	0.0002	0.0013	0.0403	0.0003	0.0010	0.0007	0.0001	0.96	0.00	0.00	14.04
5-5	0.0045	0.0036	0.0004	0.0023	0.0007	0.0001	0.0006	0.0100	0.0001	0.0003	0.0002	0.0001	0.08	0.00	0.00	1.16

5-7	0.0053	0.0064	0.0010	0.0049	0.0007	0.0001	0.0006	0.0080	0.0001	0.0003	0.0002	0.0000	0.17	0.00	0.00	3.46

lipid biomarkers

New ID	Li	Ca	Sc	Ti	V	Mn	Co	Ni	Cu	Zn	Rb	Sr	Zr	Mo	Ba
1-1	27.9	19,749	0.12	13.04	1.41	24.6	0.22	2.18	2.74	13.5	1.40	77.2	0.46	0.42	634
1-2	21.7	13,741	0.10	16.99	2.61	8.3	0.29	2.60	2.38	10.1	1.01	51.9	1.04	0.52	38.0
1-3	10.1	10,002	0.10	17.58	1.96	5.9	0.15	1.17	0.94	6.5	0.68	183	0.27	0.14	8.7
2-1	17.1	9,828	0.12	26.06	1.91	15.4	0.36	1.56	4.48	10.2	0.71	208	0.92	0.67	5.4
2-2	12.9	5,209	0.07	10.14	1.10	10.0	0.38	1.65	2.86	11.2	0.57	19.8	0.34	0.20	8.2
2-3	24.4	10,589	0.07	11.98	1.27	4.8	0.27	9.84	37.9	6.8	0.68	153	0.24	0.55	8.9
2-4	16.4	6,279	0.02	3.01	0.41	3.0	0.07	1.54	20.5	12.7	0.48	87.6	0.14	0.17	163
3-1	9.79	22,032	0.02	2.58	1.66	2.1	0.09	1.87	3.21	9.3	0.84	507	0.14	2.98	13.5
3-2	32.6	51,045	0.06	8.23	2.08	7.0	0.33	2.73	3.41	23.1	1.01	1,106	0.26	0.76	28.8
3-3	31.3	2,270	0.05	1.14	0.72	5.9	0.40	3.10	2.80	7.7	0.80	3.84	0.12	0.16	2.8

Table 3 (*continued*)

New ID	Li	Ca	Sc	Ti	V	Mn	Co	Ni	Cu	Zn	Rb	Sr	Zr	Mo	Ba
5-1	6.76	10,240	0.07	4.78	2.13	11.8	0.17	1.48	3.79	6.3	0.82	221	0.26	0.12	8.7
5-2	9.03	7,114	0.06	4.61	9.30	10.5	0.22	5.39	3.49	46.5	0.83	28	0.34	0.14	7.9
5-3	6.94	18,461	0.08	8.38	1.79	25.6	0.24	1.81	3.59	4.0	0.89	410	0.32	0.20	12.7
5-4	8.19	22,396	0.23	24.43	8.62	58.6	0.46	2.20	2.55	8.1	2.20	104	0.99	0.63	34.4
5-5	6.60	27,418	0.29	29.35	6.39	33.5	0.57	3.75	3.35	6.3	2.62	82	1.33	0.21	33.7
5-6	6.94	23,642	0.29	27.91	6.12	49.6	0.72	2.65	2.10	4.8	2.43	72	1.40	0.19	29.9
5-7	8.25	8,983	0.09	29.55	5.25	8.5	0.19	1.73	7.49	22.2	1.00	33	0.44	0.13	19.5

New ID	La	Ce	Pr	Nd	Sm	Tb	Dy	Y	Ho	Er	Yb	Lu	W	Pb	Th	U
1-1	0.38	1.00	0.10	0.36	0.07	0.01	0.05	0.35	0.01	0.03	0.03	0.00	0.04	0.47	0.13	0.47
1-2	0.38	0.97	0.09	0.34	0.07	0.01	0.06	0.43	0.01	0.04	0.04	0.01	0.04	0.66	0.14	0.44
1-3	0.44	0.88	0.09	0.36	0.06	0.01	0.03	0.20	0.01	0.02	0.01	0.00	0.01	0.51	0.13	0.19
2-1	0.37	0.82	0.09	0.37	0.07	0.01	0.06	0.32	0.01	0.03	0.02	0.00	0.01	0.27	0.06	0.24
2-2	0.21	0.57	0.05	0.22	0.05	0.01	0.04	0.26	0.01	0.02	0.02	0.00	0.02	0.59	0.04	0.12
2-3	0.19	0.36	0.05	0.20	0.04	0.01	0.04	0.32	0.01	0.02	0.02	0.00	0.05	0.39	0.03	0.11
2-4	0.08	0.16	0.02	0.09	0.02	0.00	0.01	0.10	0.00	0.01	0.01	0.00	0.01	0.24	0.01	0.05
3-1	0.06	0.18	0.01	0.07	0.01	0.00	0.01	0.05	0.00	0.00	0.00	0.00	0.02	0.39	0.01	0.30

3-2	0.66	1.41	0.14	0.59	0.09	0.01	0.04	0.23	0.01	0.02	0.01	0.00	0.03	0.86	0.06	0.99
3-3	0.14	0.38	0.04	0.16	0.04	0.00	0.03	0.20	0.01	0.02	0.02	0.00	0.02	0.29	0.02	0.08
5-1	0.20	0.42	0.05	0.19	0.04	0.00	0.03	0.17	0.01	0.01	0.01	0.00	0.02	0.30	0.07	0.15
5-2	0.15	0.35	0.04	0.14	0.03	0.00	0.02	0.12	0.00	0.01	0.01	0.00	0.03	0.21	0.04	0.03
5-3	0.35	0.59	0.08	0.33	0.06	0.01	0.04	0.23	0.01	0.02	0.02	0.00	0.04	0.38	0.08	0.39
5-4	0.65	1.24	0.16	0.60	0.12	0.01	0.09	0.62	0.02	0.05	0.05	0.01	0.08	0.62	0.18	0.42
5-5	0.88	1.69	0.21	0.81	0.16	0.02	0.12	0.81	0.03	0.07	0.06	0.01	0.02	0.89	0.22	0.08
5-6	1.00	1.86	0.24	0.95	0.19	0.02	0.17	1.10	0.03	0.09	0.08	0.01	0.01	0.95	0.24	0.21
5-7	0.40	0.80	0.09	0.34	0.07	0.01	0.05	0.30	0.01	0.03	0.02	0.00	0.01	0.37	0.08	0.09

Table 4 Lipid biomarker results

Sites	Study locations	New ID	Archaeal lipids (mg/kg dw)					
			Pytane + Crocetane	PMI	PMI:3	Archaeol	*sn*-2-hydroxyarchaeol	*sn*-3-hydroxyarchaeol
1	Congo Fan	1-1	-	-	-	0.01	0.03	-
		1-2	-	-	-	0.03	0.04	-
		1-3	0.03	0.25	-	0.83	0.60	0.22
2	Nile Deep-Sea Fan	2-1	0.21	0.42	0.49	0.92	1.28	0.10
		2-2	0.08	-	-	-	-	-
		2-3	0.05	0.02	-	0.21	0.48	0.03
		2-4	0.02	0.03	-	0.36	0.46	0.21
3	Niger Fan	3-1	0.25	0.25	0.01	6.97	22.13	-
		3-2	0.07	0.05	-	0.73	1.34	0.20
		3-3	0.09	-	-	0.09	0.23	0.02
		3-4	0.13	-	-	-	-	-
4	eastern Mediterranean Sea	4-1	-	-	-	-	-	-
5	Gulf of Mexico	5-1	0.17	0.09	-	0.31	0.68	0.04
		5-2	0.25	-	-	0.02	-	-
		5-3	0.13	0.11	-	1.76	3.20	0.29
		5-4	0.15	0.14	-	1.48	3.08	0.09
		5-5	0.07	0.03	-	0.04	0.03	-
		5-6	0.06	0.04	-	0.06	0.04	-
		5-7	0.06	0.03	-	-	-	-

Table 4 (*continued*)

Sites	New ID	Bacterial lipids (mg/kg dw)												
		DGD_If	DGD_IIa	DGD_IId	*i*-C15:0	*ai*-C15:0	C16:1ω7	C16:0	C17:0	C18:1ω9	C18:1ω7	C18:0	C20:0	C22:0
1	1-1	-	-	-	-	-	-	0.16	-	-	-	0.21	-	0.04
	1-2	-	-	-	-	-	-	0.14	-	-	0.02	0.20	0.02	0.02
	1-3	0.43	0.07	0.11	0.01	-	0.01	0.64	0.05	0.01	0.01	0.88	0.02	0.03
2	2-1	0.17	0.16	0.22	0.05	0.02	0.05	0.23	0.03	0.07	0.14	0.39	0.04	0.02
	2-2	-	-	-	-	-	-	0.06	-	0.01	-	0.15	0.01	0.02
	2-3	-	-	-	-	-	0.01	0.22	-	-	0.02	0.18	0.01	0.02
	2-4	0.06	0.12	0.22	-	0.01	-	0.24	0.02	0.03	0.02	0.19	0.01	0.02
3	3-1	0.41	1.07	0.55	0.02	0.02	-	0.14	-	0.04	0.02	0.08	-	0.01
	3-2	0.04	-	-	-	0.01	-	0.35	-	0.01	0.01	0.30	0.01	0.02
	3-3	-	-	-	-	0.02	0.06	0.22	0.02	0.02	0.08	0.19	-	0.06
	3-4	-	-	-	-	0.05	0.12	0.87	0.05	0.16	-	0.78	0.02	0.02
4	4-1	-	-	-	-	-	-	0.09	-	-	-	0.11	-	0.01
5	5-1	0.12	-	-	0.05	0.06	0.09	1.99	0.14	0.09	0.14	1.61	0.05	0.07
	5-2	0.04	-	-	0.03	0.03	0.06	0.89	0.12	0.10	-	0.63	0.03	0.06
	5-3	0.21	-	-	0.05	0.03	-	0.62	0.05	0.02	0.05	0.46	0.02	0.01
	5-4	0.29	0.25	0.39	0.01	0.02	-	0.78	0.05	0.03	0.06	0.63	0.03	0.02
	5-5	-	-	-	0.02	0.02	-	0.76	0.02	0.03	0.05	0.61	0.02	0.02
	5-6	-	-	-	-	0.02	-	0.55	0.03	-	0.08	0.39	0.01	0.06
	5-7	-	-	-	-	0.02	-	0.45	0.05	0.02	0.04	0.36	0.02	0.07

"-" indicate not determined